Politecnico di Milano

SCUOLA DI INGEGNERIA INDUSTRIALE E DELL'INFORMAZIONE

Laurea Magistrale – Telecommunication Engineering

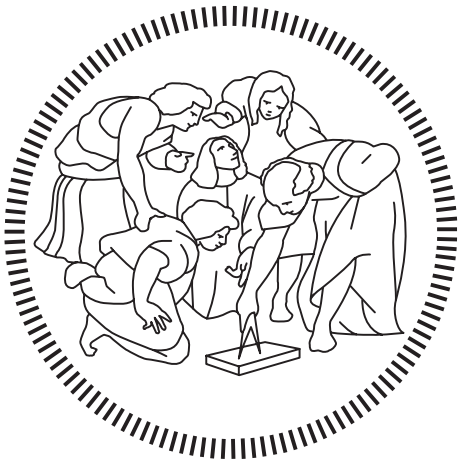

Near-field positioning for coprime arrays

Relatore

Chiar.mo Prof. Umberto SPAGNOLINI

Candidato

Marco CERAN – 970420

Anno Accademico 2021 – 2022

Acknowledgments

As my enriching experience as a Politecnico di Milano student comes to an end, I want to express my deep gratitude towards all the professors I met in my diverse and exciting learning experience, that helped me grow both on a technical and a personal level.

I also want to say thanks to all the remarkable students and friends I have had the chance to encounter in this experience, especially to Konstantinos and Giuseppe: our joint stay in Milan has been so memorable.

And finally the most heartfelt acknowledgement goes to my family: to my loving and wise parents and my affectionate and witty brothers, that have elevated and defined my life, and brought immeasurable joy to it.

Index

Abstract

Coprime arrays of antennas have seen a rise in usage in recent years due to their larger aperture, higher accuracy and higher number of degrees of freedom with respect to an Uniform Linear Arrays with the same amount of sensors. Larger aperture causes however an increase in the near-field region of the electromagnetic field around the array, making methods that rely on far-field assumption inaccurate. This poses the need for specific methods that take the curved wavefronts into account.

In this thesis, an algorithm, originally developed for far-field source direction of arrival estimation with coprime arrays has been investigated. Further, it has been modified to address the problem of near-field source direction of arrival and distance estimation with coprime arrays. This algorithm is a variation of the MUSIC algorithm for sparse array topologies that is very simple and powerful, but it has limitations on the number of the degrees of freedom of the system. The modifications made to the algorithm were in the definition of the spatial spectrum for source location. The Cramér-Rao lower-bound (CRB) of the two methods is defined.

In practical context it's shown that the method can attain the CRB in a variety of different conditions.

Keywords: coprime array, ULA, near-field, direction of arrival estimation, distance estimation, Fraunhofer distance.

Abstract in lingua italiana

Le schiere (array) coprime di antenne hanno suscitato particolare interesse negli ultimi anni per la loro maggiore apertura, miglior precisione e numero maggiore di gradi di libertà in confronto alle schiere lineari uniformi a parità di numero di antenne. L'apertura maggiore comporta un aumento delle dimensioni della regione di campo vicino intorno la schiera, invalidando i modelli basati sulle assunzioni di campo lontano. Emerge pertanto la necessità di metodi ad hoc che tengono conto della curvatura dei fronti d'onda ricevuti dalla schiera di antenne.

In questa tesi, un algoritmo, originalmente sviluppato per la stima della direzione di arrivo di segnali provenienti da sorgenti in campo lontano con schiere sparse di antenne è stato investigato. Successivamente, è stato modificato per risolvere il problema della stima della direzione di arrivo e della distanza di sorgenti in campo vicino usando schiere coprime. Questo algoritmo è una variazione del metodo MUSIC (multiple classification of signals) che è semplice e accurato, ma è capace di risolvere meno sorgenti rispetto ad algoritmi funzionanti nel dominio del difference-coarray. Le modifiche apportate all'algoritmo riguardano la definizione dello spettro spaziale del rumore. Il limite inferiore di Cramér-Rao (CRB) è stato ricavato per lo scenario sotto esame.

In contesto simulativo viene mostrato come il metodo proposto raggiunge il CRB in una varietà di condizioni analizzate.

Parole chiave: schiere coprime di antenne, schiere uniformi lineari, campo vicino, stima della direzione di arrivo, stima della distanza, distanza di Fraunhofer.

Figure list

Chapter 1

Problem definition and theoretical background

1.1 Problem definition

This thesis considers the problem of estimation of the direction of arrival and range of source signals in communication systems with the use of coprime arrays in case the sources are located in the near field of the array. This setting enables accurate location of sources located in the near-field of the array. Accuracy decreases for far-field sources as a consequence of the decreasing accuracy of distance estimation.

Direction of Arrival (DoA) estimation is a crucial problem in communication systems that use antenna arrays. It refers to the process of determining the direction from which a signal originates [1].

DoA estimation provides relevant information about the location of the signal source and helps to improve the performance of communication systems. In wireless communication systems, accurate DoA estimation can lead to better

signal quality and reduced interference by reducing the interference from other sources, resulting in improved communication performance and increased efficiency.

DoA estimation is used in various applications such as radar systems, satellite communication systems, wireless communication systems, and sonar systems. Additionally, DoA estimation is also used in localization and tracking applications, which are critical in various fields such as surveillance, navigation, and military applications.

Range (or distance) estimation is an important problem in communication and sensing system, it consists in estimating the distance between the source from which a source originates and the receiving antenna system.

Joint estimation of DoA and distance of a source enables the unambiguous computation of its positioning, allowing the system to gather useful information about the sorrounding environment.

An antenna array is a collection of multiple antennas that are combined in space to form a single system for transmitting or receiving signals. The antennas in an array are positioned in such a way that their individual signals can be combined to form a single, more powerful signal.

An Uniform Linear Array (ULA) is characterized by antennas evenly spaced along a line. In an ULA, the antennas are positioned equidistantly from one another, and the spacing between them is typically half the wavelength of the signal. The use of ULAs enables the estimation of the direction of arrival of a

signal by analyzing the phase differences between the signals received at each antenna. ULAs are the simplest and most widely adopted array topology.

A coprime array is a type of antenna array that has non-uniform spacing between its antennas. Unlike ULA, where the spacing is uniform, in coprime arrays, the spacing between the antennas is chosen such that no two antennas have distances with a common factor, except for 1. This non-uniform spacing helps to reduce the limitations of ULA, such as reduced directionality and limited angular resolution, making coprime arrays suitable for use in direction of arrival estimation applications.

The aperture D of a linear array of antennas is defined as the distance between the first and last element of the array along the axis in which the array lies.

Since an antenna array is able to detect and communicate with sources in different position, the aperture that a source actually sees is called effective aperture, and it's of course maximum in the zenith of the array, the effective aperture can be stated as:

$$D_{eff} = D \cos(\theta)$$

With θ being the incoming wave direction of arrival. The effective aperture for different impinging wave angles can be observed in figure 1.1.1

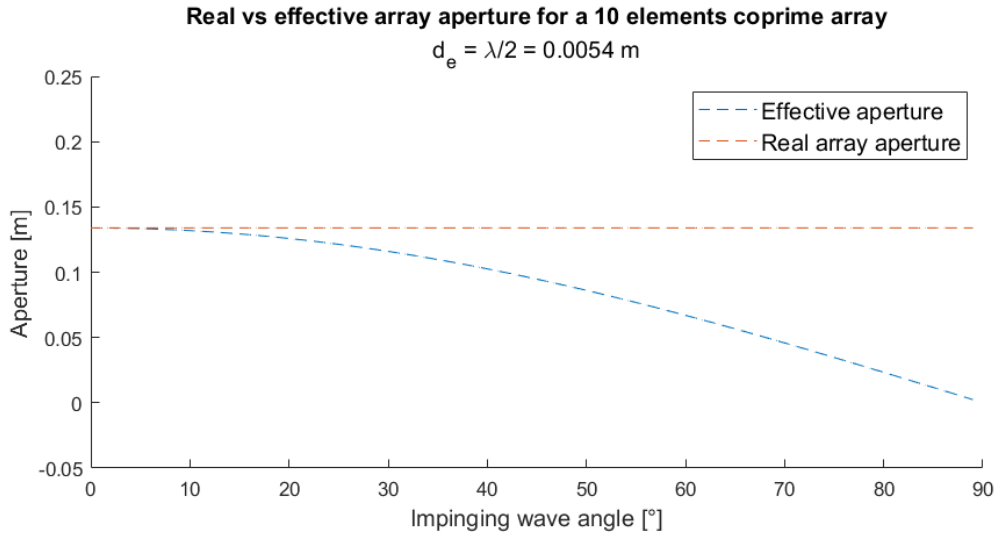

Figure 1.1.1 - Effective aperture vs impinging wave angle

1.2 Coprime array architecture

Coprime array architectures are rising in popularity because of some advantages they have over the more traditional ULA architecture, these reasons include:

- Wider aperture for a fixed number of elements w.r.t. ULA: this leads to cost savings and higher angular resolution in accordance to the Rayleigh criterion, because (λ is carrier wavelength, D is the aperture, θ is the impinging wave angle):

$$\Delta\theta_{min} \cong \frac{\lambda}{Dcos\theta}$$

- Higher number of available degrees of freedom (DoFs), i.e. number of target that can be resolved, that are N-1 for an ULA of N elements, while a coprime array of N+M-1 elements can solve up to $O(NM)$ elements.
- Enhanced resolution in direction of arrival estimation thanks to the larger aperture w.r.t. ULAs, that allows the system to distinctly resolve closely spaced sources.

Coprime arrays are made by the super-position of two sparse ULAs (ULAs with inter-element spacing > d_e = λ/2): one with N elements distanced at Md_e, the other one with M elements distanced at Nd_e, M and N being coprime integers.

In figure 1.2.1 a coprime array of 10 elements is shown, with $M = 5$, $N = 6$ being the chosen pair of coprime integer. The two sparse (aliased) ULAs that form the array are also shown, and an ULA with the same number of elements as the coprime array is shown for comparison.

Throughout this thesis arrays and sources will lie on the same plane, and the problem of DoA estimation will be solved on a 2-dimensional plane. DoA estimation results for coprime arrays are always going to be compared with results for an ULA with the same number of elements to show strengths and limitations of each array topology.

Throughout this thesis arrays and sources will lie on the same plane, and the problem of DoA estimation will be solved on a 2-dimensional plane. DoA estimation results for coprime arrays are always going to be compared with results for an ULA with the same number of elements to show strengths and limitations of each array topology.

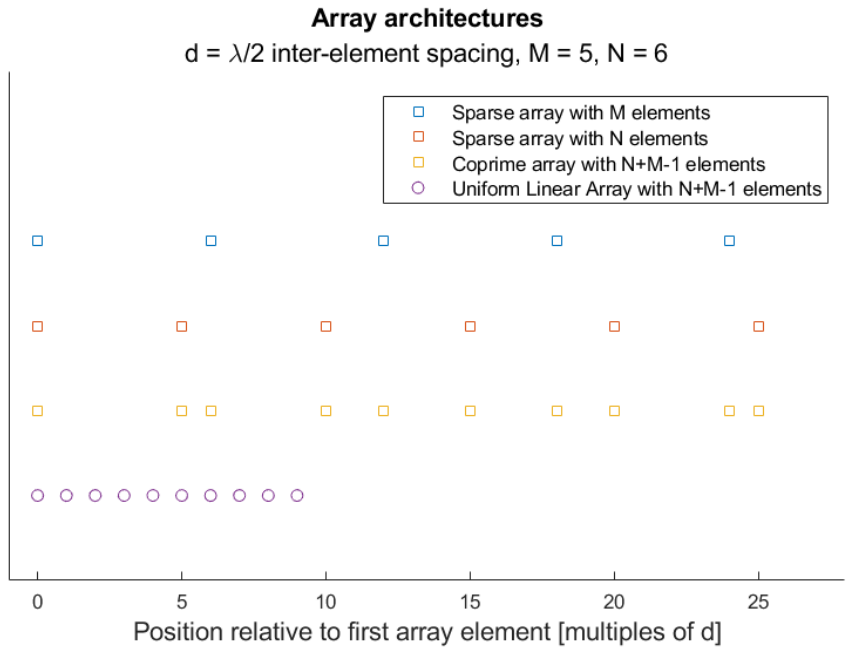

Figure 1.2.1 - ULA and Coprime array architectures

Consider a 2-dimensional cartesian coordinate system: a coprime array is located on the x-axis, the average of the elements positions along the x-axis being zero. An ULA with the same number of element is also located on the x-axis and centered around zero. These arrays topologies and positions in the xy-plane are thus shown in figure 1.2.2.

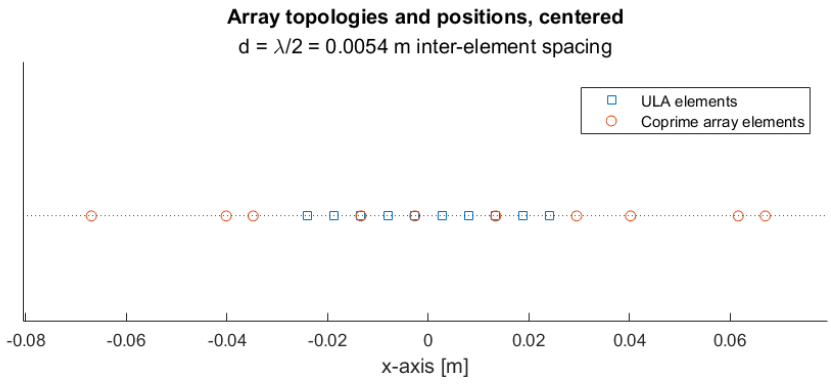

Figure 1.2.2 - Centered ULA and coprime array

Sources lie on the same xy-plane, with varying distances and angles from the origin, as shown in figure 1.2.3. The array aperture is small compared to the near-field size, this causes the array elements to appear almost superimposed in the origin of the xy axis.

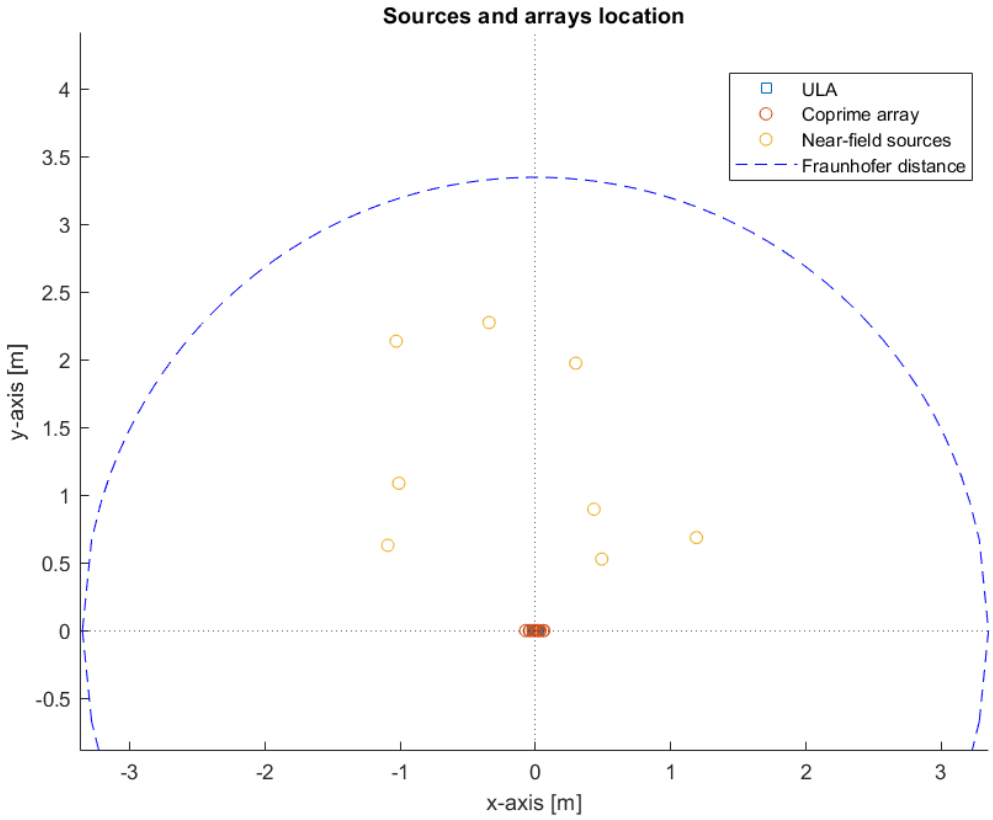

Figure 1.2.3 - Near-field sources' position with respect to array

Since this thesis revolves around sources in near-field, we will consider mostly sources with distance from the array smaller than the Fraunhofer distance of the coprime array. Fraunhofer distance is defined as:

$$d_F = \frac{2D^2}{\lambda}$$

Where D is the total array aperture, and λ is the carrier wavelength. This distance is required in order for the phase difference not to be bigger than $\pi/8$ rad (or $\lambda/16$ wavelength) at a point in space from any point in the receiving array aperture.

For a given number of elements the coprime array has a larger aperture compared to an ULA, as its elements are more spread out in space, and its d_F is consequently larger. In this thesis d_F always refers to the coprime array's Fraunhofer distance, not the ULA's one.

This criterion is therefore used to discriminate between far-field and near-field, because errors smaller than $\pi/8$ rad can be considered small enough to be negligible [2], it's also clear with this definition that the near-field of an array grows quadratically with the frequency at which it operates.

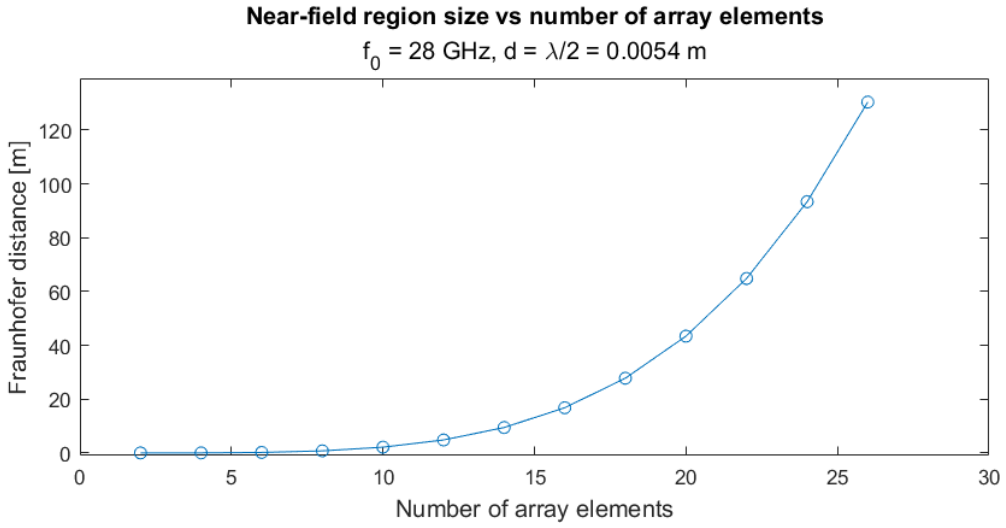

Figure 1.2.4 - Fraunhofer distance vs number of coprime array elements

In addition to that, distances are often going to be expressed as fractions of d_F, in order to better convey the idea of the Fraunhofer distance being the boundary between near-field and far-field. The typical far-field approximation models widely employed in the array processing literature can be obtained asymptotically from the more general and accurate near-field model. Figure figure 1.2.4 shows the Fraunhofer distance for coprime arrays with varying number of elements and inter element distancing $d_e = 0.0054\ m$.

1.3 Signal model

Signals emitted by the sources $\boldsymbol{s}(t)$ are typically considered nuisance parameters in line spectrum analysis, and both a deterministic modeling of the signal as well as a stochastic one are possible: the latter model is the one that is employed in this thesis.

The signal received at each time instant by the array is modeled as:

$$\boldsymbol{y}(t) = \boldsymbol{A}\boldsymbol{s}(t) + \boldsymbol{n}(t) \in \mathbb{C}^{N+M-1\times 1}$$

in which $\boldsymbol{A} \in \mathbb{C}^{N+M-1\times K}$ is the steering matrix of the array, $\boldsymbol{s}(t) \in \mathbb{C}^{K\times 1}$ are the signals impinging from the K sources on the array and $\boldsymbol{n}(t) \in \mathbb{C}^{N+M-1\times 1}$ is the noise term, assumed to be zero-mean, uncorrelated, complex and normally distributed:

$$\boldsymbol{n}(t) \sim \mathcal{CN}(\boldsymbol{0},\ \sigma_n^2 \boldsymbol{I}) \in \mathbb{C}^{N+M-1\times 1}$$

With σ_n^2 being noise power.

The signal $\boldsymbol{s}(t)$ is assumed to be stochastic and normally distributed according to:

$$\boldsymbol{s}(t) \sim \mathcal{CN}(\boldsymbol{0}, \boldsymbol{R_s})$$

In which $\boldsymbol{R_s}$ is the signal covariance matrix (a diagonal matrix because sources are uncorrelated), that is $\boldsymbol{R_s} = diag(\boldsymbol{\sigma}_s^2)$, with $\boldsymbol{\sigma}_s^2$ being the power vector of the K sources:

$$\boldsymbol{\sigma}_s^2 = [\sigma_1^2,\ \sigma_2^2,\ \ \ldots, \sigma_K^2]^T$$

Received signal can therefore be represented as:

$$\boldsymbol{y}(t) \sim \mathcal{CN}(\boldsymbol{0}, \boldsymbol{R_y})$$

With covariance matrix:

$$\boldsymbol{R_y} = \boldsymbol{A}\boldsymbol{R_s}\boldsymbol{A^T} + \sigma_n^2\boldsymbol{I} \in \mathbb{C}^{N+M-1 \times N+M-1}$$

While the signal $\boldsymbol{s}(t)$ is random and uncorrelated, $\boldsymbol{y}(t)$ is random with spatial correlation between signals received by different antenna elements that depends, among other things, on the array topology and the direction of arrival of the received signals.

A one-way communication scenario is assumed, i.e. electromagnetic waves are emitted from sources and travel to the base-station array.

The sources are assumed to be isotropical radiators, that transmit signals on a carrier wave of $f_0 = 28\ GHz$, that means having a wavelength:

$$\lambda = \frac{\mathrm{c}}{f_0} = 10.714 \cdot 10^{-3} m$$

In order to model received power ideal free-space line-of-sight trasmission is assumed, hence Friis equation is used:

$$P_r = P_t G_t G_r \left(\frac{\lambda}{4\pi R}\right)^2$$

In which:

- P_r and P_t are received and transmitted power;
- G_r and G_t are receiving and transmitting antenna gain;
- R is Tx-Rx antenna distance;
- λ is carrier wavelength.

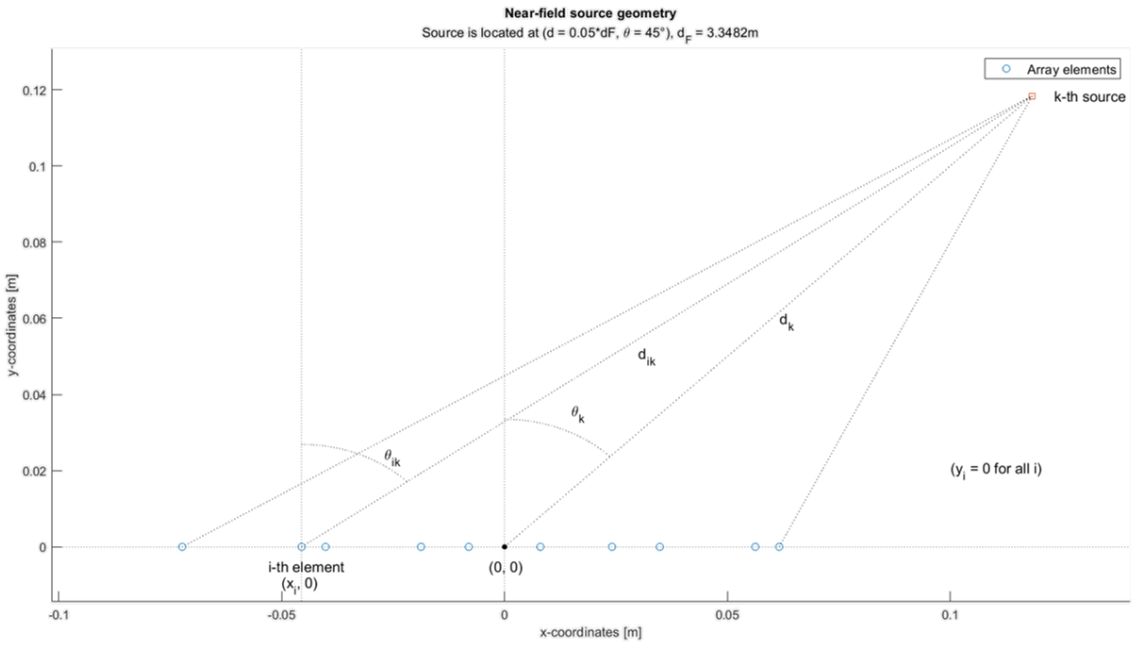

Figure 1.3.1 - Near-field sources geometry

Given this link budget model, a certain power is assigned to each source, the difference in power for each source are dependent on the distance of that source, since source transmitted power, Tx and Rx antenna gain and wavelength are constant for every source.

The K sources we are considering are impinging from angles:

$$\boldsymbol{\theta} = [\theta_1, \theta_2, \dots, \theta_K]^T$$

Since sources are located in near-field we have the geometry shown in figure 1.3.1, in which it is visible that each array element sees each source from a different angle, hence angles can be represented in $N \times K$ matrix form instead of as a $K \times 1$ vector, where the element at i-th row and k-th column is the angle:

$$\theta_{ik} = arctan\left(\frac{d_k\, sin(\theta_k) - x_i}{d_k\, cos(\theta_k)}\right)$$

The y_i term is neglected in the above formulation because array elements lay on the x-axis, and the (d_k, θ_k) pair denotes distance and angle of the source relative to the origin of the xy-plane.

In a similar way, each array element sees each source at a different distance when we are assuming near-field, because in the far-field assumption array elements are assumed to be co-located.

Therefore we can define the array-sources distances as a $N + M - 1 \times K$ matrix with elements defined by Pythagoras' theorem:

$$d_{ik} = \sqrt{(d_k\, sin(\theta_k) - x_i)^2 + (d_k \cos(\theta_k))^2}$$

As a consequence of that each element will receive a different power from each source ($\propto \frac{1}{d_{ik}^2}$).

We call $\boldsymbol{n}_e$ the vector of positions of the coprime array elements relative to the first elements, measured in multiples of the Shannon-Nyquist inter-element array spacing d_e:

$$\boldsymbol{n}_e = [n_e[1], n_e[2], \dots, n_e[N+M-1]]^T = [0,\ N,\ M,\ 2N,\ 2M,\ \dots,\ (N-1)M]^T$$

The steering matrix $\boldsymbol{A}$ is an $N + M - 1 \times K$ matrix.

When assuming flat wavefronts (far-field sources) it's defined as:

$$\boldsymbol{A}[\boldsymbol{\theta}] = \begin{bmatrix} \exp\left(j2\pi\frac{f_0}{c}d_e n_e[1]\sin(\theta_1)\right) & \cdots & \exp\left(j2\pi\frac{f_0}{c}d_e n_e[1]\sin(\theta_K)\right) \\ \vdots & \ddots & \vdots \\ \exp\left(j2\pi\frac{f_0}{c}d_e n_e[N+M-1]\sin(\theta_1)\right) & \cdots & \exp\left(j2\pi\frac{f_0}{c}d_e n_e[N+M-1]\sin(\theta_K)\right) \end{bmatrix}$$

Array elements are assumed to be isotropical radiators throughout the thesis.

Since we are working with curved wavefronts (near-field sources), steering matrix must be rewritten in order to be coherent with that.

We have defined for flat wavefronts (far-field case) the steering matrix to have the element at row i, column k equal:

$$\boldsymbol{A}_{ik} = \exp\left(j2\pi\frac{f_0}{c}d_e n_e[i]\sin(\theta_k)\right)$$

Where n_{ei} is the integer position of the i-th element, while θ_k is the angle of the k-th source with respect to the base station (assumed to be co-located in the origin).

For curved wavefronts the steering matrix has instead the element at row i, column k equal:

$$\boldsymbol{A}_{ik} = \frac{d_k}{d_{ik}} \exp\left(j2\pi \frac{f_0}{c} d_e n_e[i] \sin(\theta_{ik})\right)$$

Where:

- $n_e[i]$ is the integer position of the i-th element;
- θ_{ik} is the angle of the k-th source with respect to the i-th array elements;
- d_k is the distance from k-th source from the origin (the array is centered in the origin);
- d_{ik} is the distance from the k-th source to the i-th array element.

The d_k/d_{ik} ratio represents the different received power between an hypotetical element in the origin of the axes, whose distance from the transmitting source is d_k, and the actual power received by the i-th element d_{ik}, this ratio is neglected ($d_k/d_{ik} = 1$) in the far-field model, since array elements are assumed to be co-located [3].

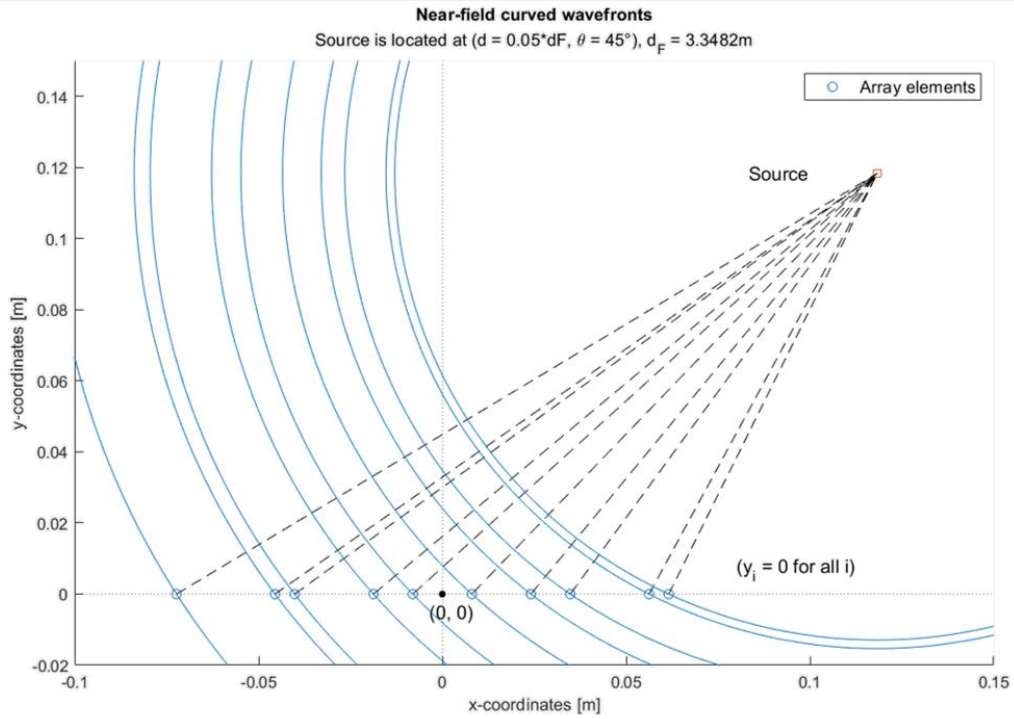

Figure 1.3.2 - Curved wavefronts for near-field sources

In figure 1.3.2 curved wavefronts are graphically shown for a source located at $(d = 0.05d_F, \theta = 45°)$.

Sources are assumed to be narrowband, i.e. $f_0 \gg B$ (B being sources' bandwidth) [4], in narrowband signals, the signal envelope is so smooth that it does not change significantly within some cycle of carrier sinuoids:

$$s(t-\bar{\tau})e^{j2\pi f_0(t-\bar{\tau})} \simeq s(t)e^{j2\pi f_0(t-\bar{\tau})}$$

With $\bar{\tau}$ being a delay of some periods of the carrier sinusoid (it's assumed that $|\bar{\tau}| \ll 100/f_0$).

The array samples the received signal at intervals $t \in \{0, \pm\Delta t, \pm 2\Delta t, \dots\}$ with $\Delta t = \frac{1}{2B}$ in order to avoid aliasing, in compliance with the Shannon-Nyquist sampling

theorem, and the samples (snapshots) collected at these time intervals are assumed to be random and uncorrelated in time, so that:

$$\mathbb{E}\left[\boldsymbol{y}(n\Delta t)\boldsymbol{y}^{\boldsymbol{H}}\left((n+k)\Delta t\right)\right] = \begin{cases} \boldsymbol{A}\boldsymbol{R}_{\boldsymbol{s}}\boldsymbol{A}^{\boldsymbol{H}} + \sigma_n^2\boldsymbol{I} & \text{for k} = 0 \\ 0 & \text{for k} \neq 0 \end{cases}$$

From these snapshots we can compute the sample covariance matrix:

$$\widehat{\boldsymbol{R}}_{\boldsymbol{y}} = \frac{1}{T}\sum_{t=1}^{T} \boldsymbol{y}(t)\boldsymbol{y}^{H}(t)$$

That converges to the true covariance matrix for number of snapshots $T \to \infty$.

1.4 Beamforming – Far-Field

Beamforming, or spatial filtering is a signal processing technique that combines elements in the antenna array in such a way that signals at particular angles experience constructive interference while others experience destructive interference [5].

With this procedure we are able to increase the system SNR by adding signals coherently and noise incoherently, this improvement is measured by the array gain.

Spatial frequency beamforming works by performing a weighted sum (with complex weights) of the different signals received at the various array elements

in order to obtain a signal coming from a specific direction, as opposed to time delay based techniques like delay-and-sum beamforming.

The beamformer complex coefficients, when assuming far-field sources, take the form of a steering vector equivalent to the one previously stated:

$$\boldsymbol{a}[\theta] = \left[\exp\left(j2\pi\frac{f_0}{c}d_e n_e[1]\sin(\theta)\right) \quad \dots \quad \exp\left(j2\pi\frac{f_0}{c}d_e n_e[N+M-1]\sin(\theta)\right)\right]^T$$

Since the array element in this thesis are considered to be unitary gain isotropical radiators, the array gain equals the radiation pattern of the array (since the radiation pattern is the product of array gain and element radiation pattern).

Half power beamwidth (or HPBW) is a standard parameter that measures the performance of an antenna array by its radiation pattern, and it's used to quantify the bandwidth, or selectiveness, of a spatial filter.

HPBW is defined as an angular width, measured on the major lobe of the antenna radiation pattern, of the portion of the pattern with attenuation lower than 3 dB (half power, hence the name) compared to the peak.

Low HPBW values are desirable in antenna arrays in order to have more selective spatial filters. HPBW is lower in arrays with more elements and/or higher aperture, therefore coprime array have a lower HPBW in comparison to ULAs for a fixed number of elements.

In figure 1.4.1 are shown radiation patterns for 10 element coprime arrays and ULAs with beams pointing at 0°, 15°, 30°, 45°, 60° and 75° respectively.

Coprime array have narrower main lobes, that allows them to be more selective then ULAs.

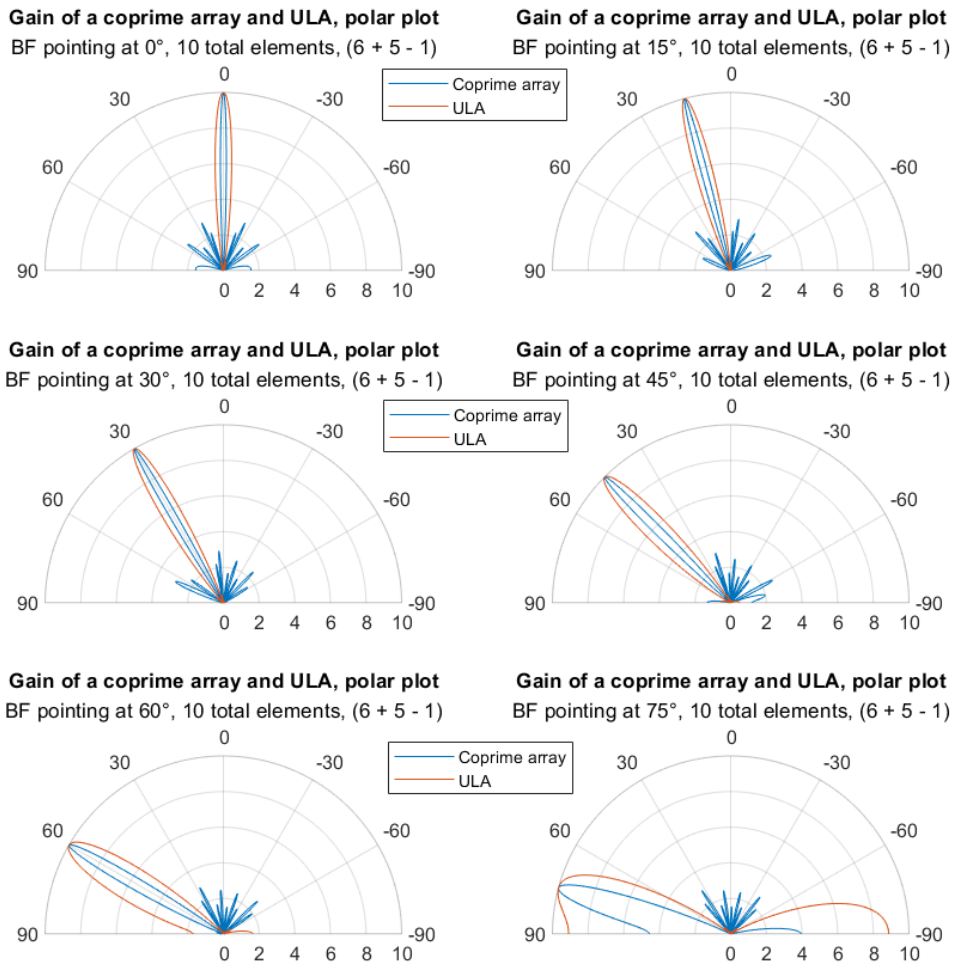

Figure 1.4.1 - Far-field radiation pattern of coprime arrays and ULAs of isotropical antennas with varying beamformer angle

Predictably the HPBW is higher when the beamformer points towards more angled directions (farther from 0°).

The figure 1.4.2 shows the HPBW vs beamformer angle for a coprime array and an ULA of 10 elements, the fact that the lowest HPBW is registered when the beamformer points at 0° is due to the fact the effective aperture is maximum when a source is at 0°, and it diminishes gradually with more angled source locations. The HPBW vs beamformer angle plot is naturally symmetric in 0°.

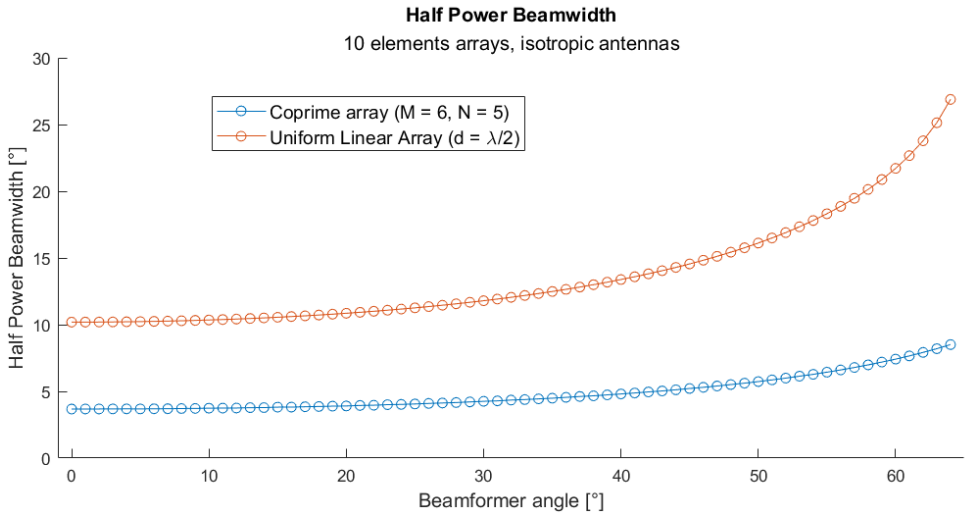

Figure 1.4.2- Half-power beamwidth vs beamformer angle for coprime array and ULA

1.5 Beamforming – Near Field

Since this thesis revolves around the direction of arrival estimation of sources in the near field of the antenna array, the previously stated far-field beamformer cannot be used, instead a near field formulation has to take curved wavefronts into account.

This near-field beamformer is a function of two parameters, distance and direction of arrival, for geometrical reasons already stated, as opposed to the far-field beamformer that solely depends on the direction.

This beamformer's coefficients take the form:

$$\boldsymbol{a}_i[d,\theta\,] = \frac{d}{d_i}\exp\left(j2\pi\frac{f_0}{c}d_e n_e[i]\sin(\theta_i)\right)$$

Where:

$$\theta_i = arctan\left(\frac{d\,sin(\theta) - x_i}{d\,cos(\theta)}\right)$$

and

$$d_i = \sqrt{(d\,sin(\theta) - x_i)^2 + (d\cos(\theta))^2}$$

are equivalent to the already described formulations for angle and distance from each array element to the point in space to which the beamformer is pointing.

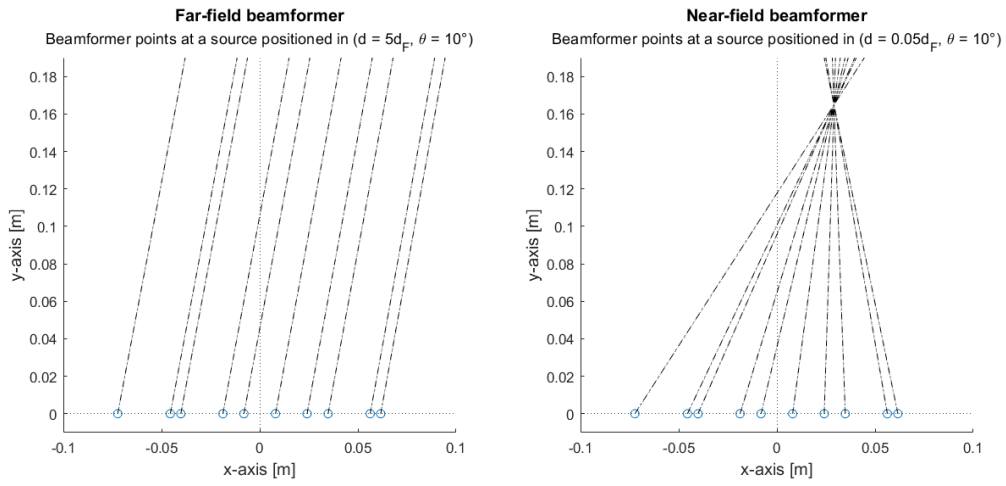

Figure 1.5.1 - Directions pointed by a beamformer in far-field and in near-field

The d/d_i ratio accounts for the different power received by each antenna element as a consequence of the variations in source-element distances, with d being the source's distance from the origin of the axes.

Instead of pointing to all sources in a given direction, this beamformer formulation points to a specific point in the 2D plane, represented by its polar coordinates, as shown in an example in figure 1.5.1.

Chapter 2

Proposed localization algorithm

2.1 The Direct MUSIC Method

MUSIC (MUltiple SIgnal Classification) [1] is an algorithm used for frequency estimation and radio direction finding.

The algorithm inputs the covariance matrix $\boldsymbol{R_y}$ of the signals as received by each antenna element, performs an eigen decomposition, separates the result into signal and noise subspaces, derives an angular spectrum from this information, and finally searches that spectrum for peaks that represent signal arrival angles.

It's a subspace method based on the property that the first K eigenvectors associated with the leading (in descending order) eigenvalues of $\boldsymbol{R_y}$ are a basis of the columns of the steering matrix associated to the sources and the array of antennas previously illustrated.

Those subspace properties can be extended to the sample correlation matrix $\widehat{\boldsymbol{R}}_{\boldsymbol{y}}$. Let the eigenvector decomposition be $\widehat{\boldsymbol{R}}_{\boldsymbol{y}} = \widehat{\boldsymbol{Q}}\widehat{\boldsymbol{\Lambda}}\widehat{\boldsymbol{Q}}^{\boldsymbol{H}}$, the K eigenvectors $\widehat{\boldsymbol{Q}}_s = [\widehat{\boldsymbol{q}}_1, \widehat{\boldsymbol{q}}_2, \dots, \widehat{\boldsymbol{q}}_K]$ associated to the leading eigenvalues span the signal subspace:

$$\mathcal{R}(\widehat{\boldsymbol{Q}}_S) \approx \mathcal{R}(\boldsymbol{A}(\boldsymbol{\theta}))$$

And equivalently, the remaining eigenvectors form an $(N+M-1)\times(N+M-1-K)$ matrix $\widehat{\boldsymbol{Q}}_N = [\widehat{\boldsymbol{q}}_{K+1}, \widehat{\boldsymbol{q}}_{K+2}, \dots, \widehat{\boldsymbol{q}}_{N+M-1}]$ that spans the noise subspace:

$$\mathcal{R}(\widehat{\boldsymbol{Q}}_N) \approx \mathcal{N}(\boldsymbol{A}(\boldsymbol{\theta})^{\boldsymbol{H}})$$

The $\approx$ symbol is used to highlight that the equality is exact only asymptotically for $T \to \infty$.

Therefore $\widehat{\boldsymbol{Q}}_S$ is the basis of the signal subspace and $\widehat{\boldsymbol{Q}}_N$ is the complementary basis of the noise subspace drawn from the limited T observations.

From the decomposition, the orthogonality condition follows:

$$\boldsymbol{A}(\boldsymbol{\theta})^{\boldsymbol{H}}\widehat{\boldsymbol{Q}}_N \approx \mathbf{0}$$

So we have that for each direction:

$$\boldsymbol{a}(\theta)^{\boldsymbol{H}}\widehat{\boldsymbol{Q}}_N\widehat{\boldsymbol{Q}}_N{}^{\boldsymbol{H}}\boldsymbol{a}(\theta) \approx \mathbf{0} \text{ for } \theta = \theta_1, \theta_2, \dots, \theta_L$$

The noise spectrum can be thus obtained using a trial steering vector $\boldsymbol{a}[\theta]$ as:

$$\mathcal{S}_N(\theta) = \frac{1}{\sum_{k=K+1}^{N+M-1} |\hat{q}_k^H \boldsymbol{a}(\theta)|^2} = \frac{1}{\boldsymbol{a}(\theta)^{\boldsymbol{H}}\widehat{\boldsymbol{Q}}_N\widehat{\boldsymbol{Q}}_N{}^{\boldsymbol{H}}\boldsymbol{a}(\theta)}$$

The direction of arrival are estimated as the L values of θ that maximize the noise spectrum $\mathcal{S}_N(\theta)$, in fact for those values the denominator approaches zero.

An alternative, but equivalent way to determine the sources' DoAs with the MUSIC algorithm is that of exploiting the $\widehat{\boldsymbol{Q}}_S$ matrix, basis of the signal subspace, and maximizing the signal spatial spectrum:

$$\mathcal{S}_S(\theta) = \sum_{k=K+1}^{N+M-1} |\hat{q}_k^H \boldsymbol{a}(\theta)|^2 = \boldsymbol{a}(\theta)^{\boldsymbol{H}} \widehat{\boldsymbol{Q}}_S \widehat{\boldsymbol{Q}}_S{}^{\boldsymbol{H}} \boldsymbol{a}(\theta)$$

This alternative method achieves superior performance when the $\widehat{\boldsymbol{Q}}_S$ matrix has greater size than $\widehat{\boldsymbol{Q}}_N$, i.e. when $K > N + M - 1 - K$, or equivalently when:

$$K > \frac{N + M - 1}{2}$$

While conversely the $\widehat{\boldsymbol{Q}}_N$ based method has higher performance when this condition is not satisfied.

This standard algorithm is typically employed with uniform linear arrays, but it can be generalized without loss of validity and performance to sparse array design, as shown in [6], this method is refferred to as "Direct" MUSIC throughout this work in order to highlight the fact that it is applied directly to the sample covariance matrix obtained from the signal received by the array elements from the sources as opposed to applying it to a coarray-domain reconstructed covariance matrix, as shown in [7].

In order to use this approach the steering vectors $\boldsymbol{a}(\theta)$ that are used sample the signal in space in accordance to the sparse array topology.

Sources are unambiguously identified using this method when the integer indexes of the array are coprime, i.e. when their greatest common divisor is 1. In this case the array manifold is said to be invertible, and the mapping from θ to $\boldsymbol{a}(\theta)$ is injective (one-to-one). An example of non-invertible array is one with a topology:

$$[0, M, 2M, \dots, NM]$$

with M > 1, in this case sources can be identified unambiguously only in a $2\pi/M$ interval (a phenomenon known as spatial aliasing [8]).

The Cramér-Rao lower bound can be easily computed for this near-field setting and it can be showed to be remarkably lower than that of an ULA.

However, the Direct MUSIC method with coprime arrays does not take full advantage of the increased number of degrees of freedom that this topology provides, as it's only able to solve up to N+M-2 sources for an N+M-1 elements array.

In this thesis, the number of sources is assumed to be known when computing DoAs using MUSIC, but methods to estimate source number from the received signal covariance matrix have been explored in literature [9].

2.2 Near-field direct MUSIC method

The previously illustrated method is meant for far-field sources DoA estimation, a scenario in which sources' distance is not a parameter of interest. On the other hand, when the sources are located in the near-field of the array, and the geometrical setting is the one illustrated in Section 1.5, distance can be estimated from the $\widehat{\boldsymbol{Q}}_N$ (or $\widehat{\boldsymbol{Q}}_S$) matrix too.

When using the near-field beamformer to search for sources with the coprime array the noise spectrum becomes:

$$\mathcal{S}_N(d,\theta) = \frac{1}{\sum_{k=L+1}^{N} |\hat{q}_k^H \boldsymbol{a}(d,\theta)|^2} = \frac{1}{\boldsymbol{a}(d,\theta)^{\boldsymbol{H}} \widehat{\boldsymbol{Q}}_N \widehat{\boldsymbol{Q}}_N{}^{\boldsymbol{H}} \boldsymbol{a}(d,\theta)}$$

And the noise spectrum maximization operation that is used to locate the sources becomes a 2D search.

From this 2D peak finding operation sources' location is obtained from their directions of arrival and distances. However, geometrical limitations cause ranging of sources located beyond the Fraunhofer distance to be inaccurate.

Sources' positions are obtained by combining the estimated distance and DoA, since the number K of sources is known a priori, these distances and DoA are jointly estimated as the coordinates of the peaks in the two-dimensional noise spectrum.

2.3 Peak finding method

In order to find these peaks, the $\widehat{\boldsymbol{Q}}_N$ matrix formed by the eigenvectors associated to the noise is computed from the sample covariance matrix $\widehat{\boldsymbol{R}}_{\boldsymbol{y}}$.

Then a two-dimensional grid of points corresponding to pairs of angle and distance values is defined, and the value of the near-field noise spectrum is computed for each point (that corresponds to a possible source position in the xy plane).

A position is then defined as a peak if it has a higher near-field noise spectrum value than the 4 points adjacent to it (i.e. the points immediately to the upper, lower, left and right in the grid).

This operation may produce spurious peaks, i.e. peaks that do not correspond to a source being located in that position, this phenomenon occurs especially in low SNR and small number of snapshots situations. These spurious peaks typically have lower noise spectrum values than the proper peaks that we are interested in finding, therefore the peaks are sorted by descending noise spectrum value and only the first K peaks (corresponding to the K sources that we are trying to find) are considered.

This procedure, when carried out with a sufficiently dense grid is able to yield accurate measurements of the sources position, but from a computational point of view it is an inefficient procedure, because both time and memory complexity of this algorithm grow linearly with the distance (or DoA) resolution specified when generating the grid, and they grow quadratically when increasing both distance and DoA resolution.

A way to overcome this problem is that of using a grid that has a coarse resolution, corresponding to the minimum resolution that allows the system to correctly tell apart two close sources (typically in the 10^{-1} to 10^{0} degrees range in direction), and then perform local iterative improvements to the first estimate.

This improvement method consists in, for each of the K sources' locations that have been found, defining a new grid in a local neighborhood of the position, and find a new peak in this grid. This operation can be repeated any number of

times to further improve the resolution of the peak finding algorithm, and its computational advantage lies in the fact that it's much more efficient, both from a time and memory point of view, to calculate multiple times the location of a peak in a coarse grid rather than computing one time the location of one or more peaks in a fine-grained grid, especially in high SNR and number of snapshots situation, in which the system is able to achieve very accurate estimates of sources' distances and DoA.

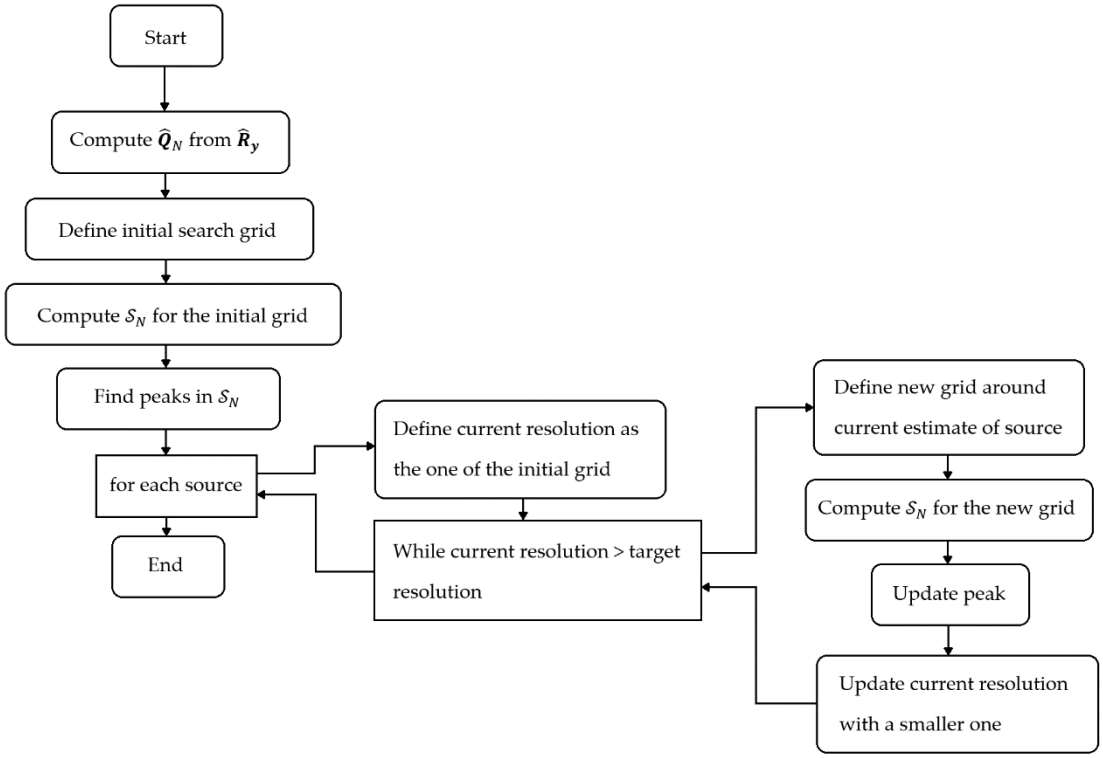

Figure 2.3.1 - Block diagram of the two-dimensional peak search algorithm to estimate direction of arrival and position from noise spectrum

In order to quantify the computational efficiency gain derived by iteratively improving coarse initial solutions instead of using a fine-grained grid from the start an example can be provided. In this scenario the goal is to estimate the position of a source with a precision of up to 10^{-5} degrees in direction and $10^{-4}\ m$ in distance, assuming sources have distance and DoA in the $[-90°,\ 90°]$ and $[0\ m, 10\ m]$ ranges respectively.

A fine-grained grid in those ranges and with those resolutions would be a $9 \cdot 10^6 \times 10^5$ matrix, resulting in a total of $9 \cdot 10^{11}$ noise spectrum computations, stored in a 7.2 TB matrix of *double* type variables in MATLAB.

On the other hand, an intial grid with granularity $0.5°$ and $0.05\ m$ results in a 361×100 matrix, that requires 36100 noise spectrum computations, stored in a 288 KB matrix of the same type as before. Assuming that each improvement iterative step is computed on a 10×10 matrix grid localized in a neighbourhood of the current estimate, just 6 improvement steps would be required for each source to meet the specified maximum precision, leading to $600 \cdot K$ additional noise spectrum computations, i.e. a total of $36100 + 600 \cdot K$ total noise spectrum computations.

Chapter 3

Cramér-Rao bound

The Cramér-Rao bound (CRB) [10][11] sets the lower value of the covariance for any unbiased estimator with a parametric probability density function that can be asymptotically attained by the ML estimator for a large number of observations [4].

The CRB can always be computed in closed form and, even if an estimator that attains it does not always exist in explicit form, it is a very informative metric to assess the accuracy of an estimation method, as no estimator can have variance lower than the CRB.

CRB is obtained from the inversion of the Fisher Information Matrix (FIM) [12], that is a way of measuring the amount of information that an observable random variable carries about an unknown parameter of a distribution that models the random variable that is observed.

Since distance and direction of arrival are jointly estimated with the near-field direct MUSIC method, the CRB is jointly derived for these two parameters, so we have a $2K \times 1$ parameter vector:

$$\boldsymbol{\xi} = [\theta_1, \dots, \theta_K, d_1, \dots, d_K]^T$$

And the CRB matrix will have the $2K \times 2K$ form:

$$\begin{bmatrix} cov_{CRB}[\hat{\theta}_1] & 0 & 0 & & & \ddots & \\ 0 & \ddots & 0 & & & & \\ 0 & 0 & cov_{CRB}[\hat{\theta}_K] & & & & \\ & & & cov_{CRB}[\hat{d}_1] & 0 & 0 & \\ & \ddots & & 0 & \ddots & 0 & \\ & & & 0 & 0 & cov_{CRB}[\hat{d}_K] & \end{bmatrix}$$

Then the FIM is therefore a $2K \times 2K$ matrix whose element at i-th row and j-th column is:

$$\boldsymbol{FIM}[i,j] = T\ tr\left(\boldsymbol{R_y^{-1}}\frac{\partial \boldsymbol{R_y}}{\partial \boldsymbol{\xi}[i]}\boldsymbol{R_y^{-1}}\frac{\partial \boldsymbol{R_y}}{\partial \boldsymbol{\xi}[j]}\right)$$

$$= T\ tr\left(\frac{\partial \boldsymbol{R_y}}{\partial \boldsymbol{\xi}[i]}\boldsymbol{R_y^{-1}}\frac{\partial \boldsymbol{R_y}}{\partial \boldsymbol{\xi}[j]}\boldsymbol{R_y^{-1}}\right)$$

$$= T\ vec\left(\frac{\partial \boldsymbol{R_y}}{\partial \boldsymbol{\xi}[i]}^H\right)^H (\boldsymbol{R_y}^{-T} \otimes \boldsymbol{R_y}^{-1}) vec\left(\frac{\partial \boldsymbol{R_y}}{\partial \boldsymbol{\xi}[j]}\right)$$

Since $\boldsymbol{\xi}$ can represent either an angle or a distance we have two cases:

$$\begin{cases} \dfrac{\partial \boldsymbol{R_y}}{\partial \theta_k} = \dfrac{\partial(\boldsymbol{A R_s A}^H + \sigma_n^2 \boldsymbol{I})}{\partial \theta_k} = \dfrac{\partial \boldsymbol{A}}{\partial \theta_k}\boldsymbol{R_s A}^H + \boldsymbol{A R_s}\dfrac{\partial \boldsymbol{A}}{\partial \theta_k}^H \\ \dfrac{\partial \boldsymbol{R_y}}{\partial d_k} = \dfrac{\partial(\boldsymbol{A R_s A}^H + \sigma_n^2 \boldsymbol{I})}{\partial d_k} = \dfrac{\partial \boldsymbol{A}}{\partial d_k}\boldsymbol{R_s A}^H + \boldsymbol{A R_s}\dfrac{\partial \boldsymbol{A}}{\partial d_k}^H \end{cases}$$

So the $\boldsymbol{CRB}$ is obtained as:

$$\boldsymbol{CRB} = \boldsymbol{FIM}^{-1}$$

and:

$$\begin{cases} CRB(\theta_k) = \boldsymbol{CRB}[i,i] & i \in [1,K] \\ CRB(d_k) = \boldsymbol{CRB}[i,i] & i \in [K+1, 2K] \end{cases}$$

This $2K \times 2K$ CRB matrix is obtained by inverting a $2K \times 2K$ FIM matrix.

In Appendix A a detailed derivation of the FIM analytical expression is reported.

This CRB formulation is based upon three assumptions:

1. Linearly independent steering vectors (each steering vector is associated to a source);
2. Additive zero-mean gaussian uncorrelated complex noise;
3. Positive-definite covariance matrix;

All three of these assumption are met in our scenario, and this CRB formulation works both with near-field and far-field steering matrixes, and works for ULAs, coprime arrays and any other sparse array architecture, as long as the array topology that is used is invertible (in the sense expressed in [6]).

The lower bounds on a source direction of arrival and distance estimator variances depend on the specific positions of the source, that is expressed by (θ_k, d_k).

In particular, CRB on source's distance estimation gets higher for sources that are farther in space from the receiving array of antennas for Geometric Dilution of Precision (GDOP) reasons, as shown in figure 3.1 and for more angled sources (in the left part the array elements are almost superimposed because $d \gg d_e$).

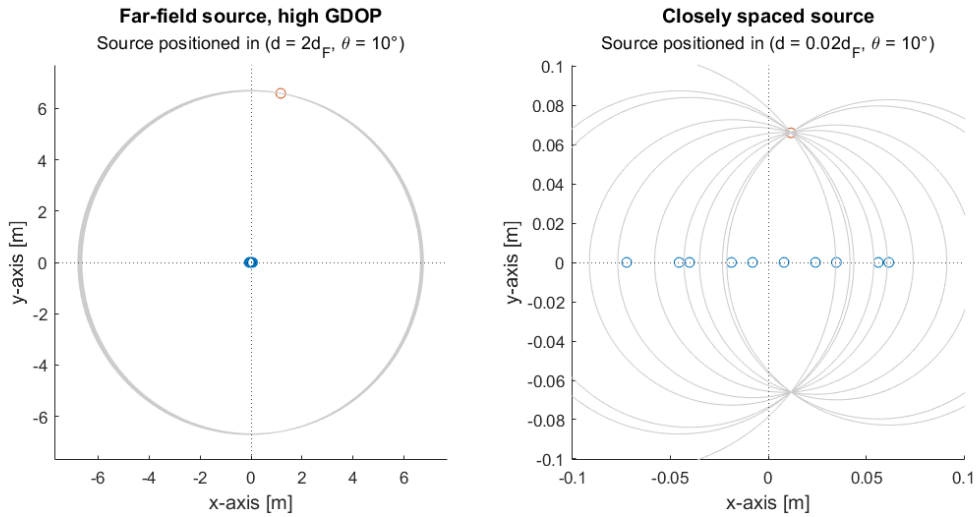

Figure 3.1 - Examples of sources with high and low GD*OP*

On the other hand, CRB on source's direction of arrival estimation does not experience great variations in performance when varying source's distance from the array, because for sources with distance greater than the Fraunhofer distance we bring us back to the (simpler) case of far-field DoA estimation. DoA estimation's performance degrades for more angled positions, because the effective aperture gets lower.

In the figure 3.2 the source position estimation's confidence regions obtained from the CRB values relative to DoA and distance estimation. The plot is relative to a 10 elements array with $T = 150$ snapshots and $SNR = 30\ dB$.

In addition to this it must be noted that the ellipses are not to scale: in fact their semiaxes have been stretched by a factor 10 in the radial direction (relative to the distance estimation), and by a factor 1000 in the tangential direction (relative to the DoA estimation), in order to make the plot more interpretable, still it's

evident by the proportion of the ellipses how the localization performance degrades for farther and more angled sources.

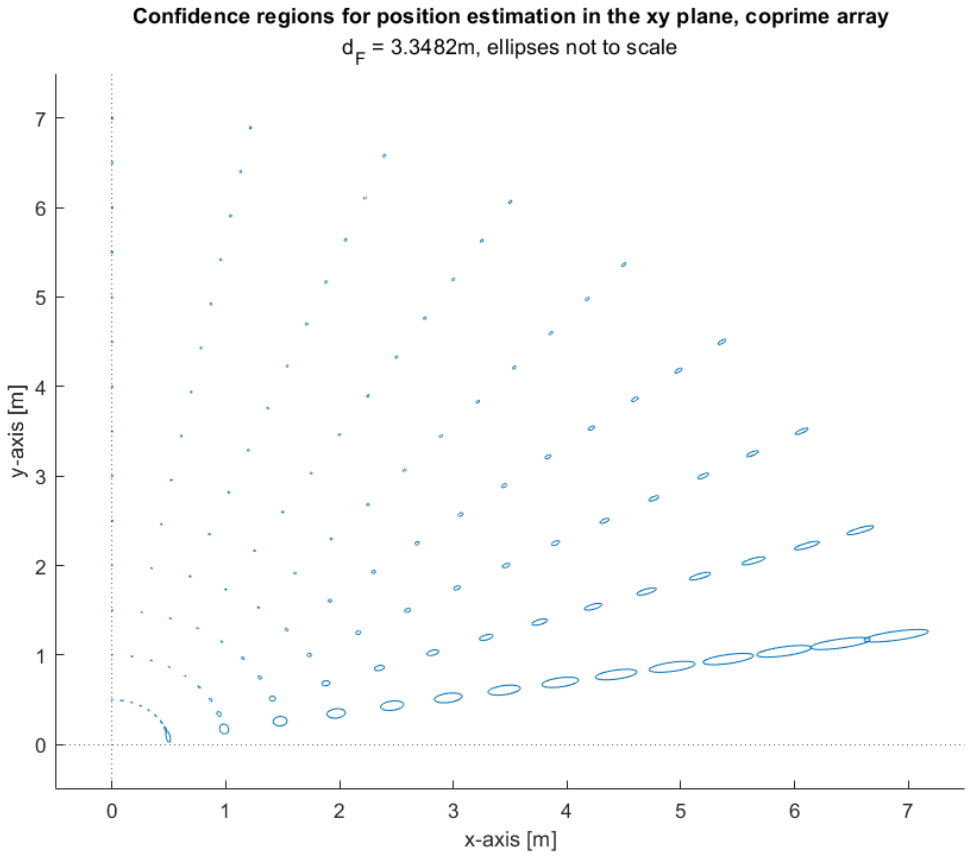

Figure 3.2 - Confidence ellipses for sources located in various position in the near and far-field of the coprime array

Chapter 4

Practical results

In this section the previously outlined method is applied in the MATLAB software environment and the simulation results are going to be reported and commented.

4.1 Mean Squared Error vs Cramér-Rao Bound

In this section results obtained from a coprime array of 10 (5+6-1) elements are going to be compared with that of an ULA with the same number of elements, and both the coprime array's and the ULA's MSE for DoA and distance estimation are compared with the respective CRB.

This method is only able to solve up to N+M-2 sources, i.e. 9 sources in our case.

Both the coprime array and the ULA are positioned along the x-axis, with the array aperture centered in the origin of the axes, sources communicate with the array on a central frequency of $f_0 = 28\ GHz$, and a bandwidth $B = 400\ MHz$. The

resulting Fraunhofer distance for the coprime array of 10 elements is $d_F = 3.348\,m$.

Sources have a transmitting power of $P = 23\,dBm = 0.2\,W$, and both the receiving and transmitting antenna have gain $G_{Rx} = G_{Tx} = 10dB$. Given these parameters, and the sources' distances from the origin, power received by the array is computed using the previously specified model (i.e. Friis equation).

The Mean Square Errors (MSE) that are reported in the following plots are expressed in dB, where an MSE of 0 dB corresponds to a RMSE of 1 rad and 1 m, or an MSE of $(1\,rad)^2 \cong 3282.8(°)^2$ and $1\,m^2$ respectively for direction and distance.

Noise power is adjusted in order to have a specific SNR that depends on the particular simulation that is carried out.

The 2D search for peaks in the near-field noise spectrum of the signal received by the array has to be computed in a grid with boundaries that have to be specified in advance: this grid has been chosen to have boundaries at $\pm 90°$ in the direction dimension, and 0 to $2d_F$ in the distance dimension, unless otherwise noted. A grid with a limited dimension in distance is chosen because most of the sources that are going to be localized lie in the near-field of the array, and having a smaller grid makes for faster computations, although poses a higher bound on the maximum MSE that is attained on the distance estimation.

In fact, when sources can be assumed to lie in a narrower interval in the distance or direction dimensions those narrower boundaries can be used instead, yielding a smaller grid that leads to more efficient computation; in the event in which no

such assumption can be made on a sound basis the distance interval can be set to be arbitrarily large, and the direction interval is set to $[-90°, +90°]$, knowing that the computation will be more complex (or less accurate), and that the distance estimation performance degrades significantly for farther sources.

The granularity of the initial grid is set to $0.5°$ and $0.05d_F$ for the DoA and distance dimensions respectively. The angular granularity of the initial search grid is an important parameter because it determines the system's ability of discerning closely spaced sources; it has been set to $0.5°$, for this has been found experimentally to be a value close to the system's angular resolution.

In order to get results that accurately depict the performance of the proposed method in spite of the intrinsic randomness that comes with stochastic signal and noise modeling, the Monte Carlo method has been used in the simulations.

Means square errors of the direction of arrival and distance estimation are treated as random variables that depend on the realizations of the stochastic processes used to represent signal and noise. Therefore, for each particular simulation, a large number of iterations have been performed, and the empirical mean of the MSE for these iterations has been taken as the MSE to be compared to the CRB.

The $MSE = (1°)^2$ and $MSE = 1\,m^2$ lines in the MSE vs CRB plots represents the MSE levels that correspond to $1°$ and $1\,m$ of RMSE respectively, and can be used as reference.

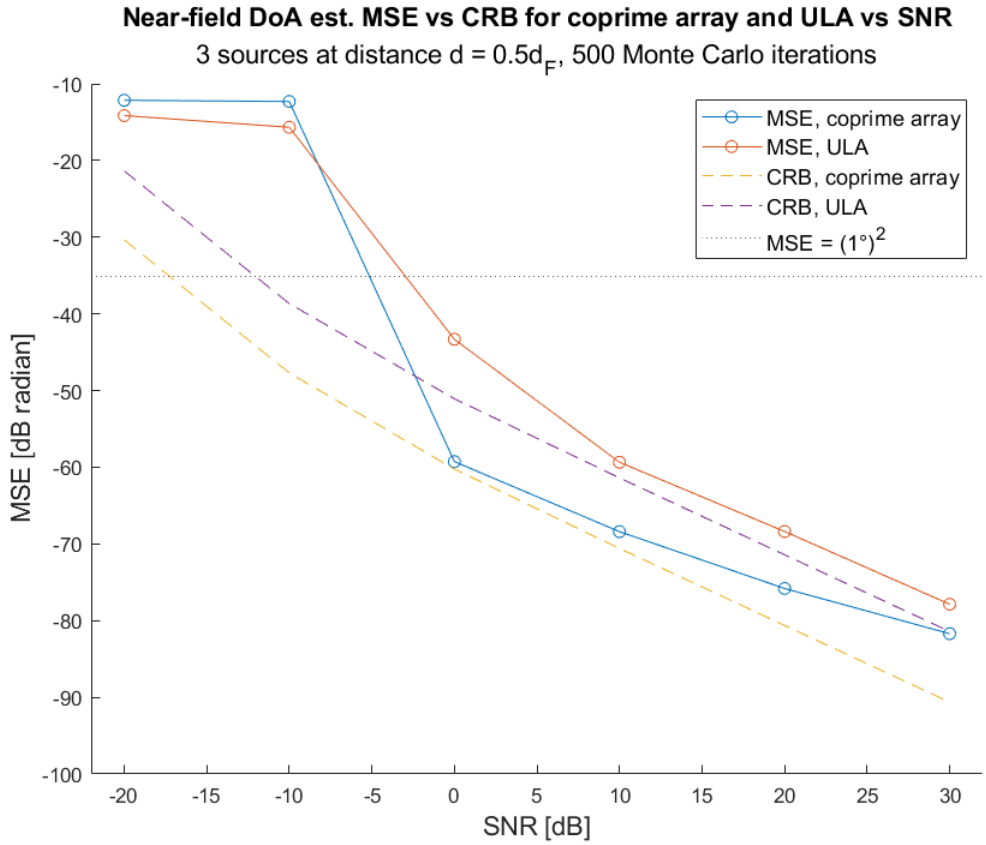

Figure 4.1.1 - DoA estimation accuracy vs Signal to Noise ratio

Figure 4.1.1 the simulation results for the direction of arrival estimation are presented for varying SNR. In this scenario a total of 500 Monte Carlo simulations have been performed, with a coprime array and an ULA, both of 10 elements, placed in the origin to estimate the DoA of 3 sources evenly spaced at [-60°, 0°, 60°], and distance $d = 0.5d_F$. The total number of snapshots has been set to 150.

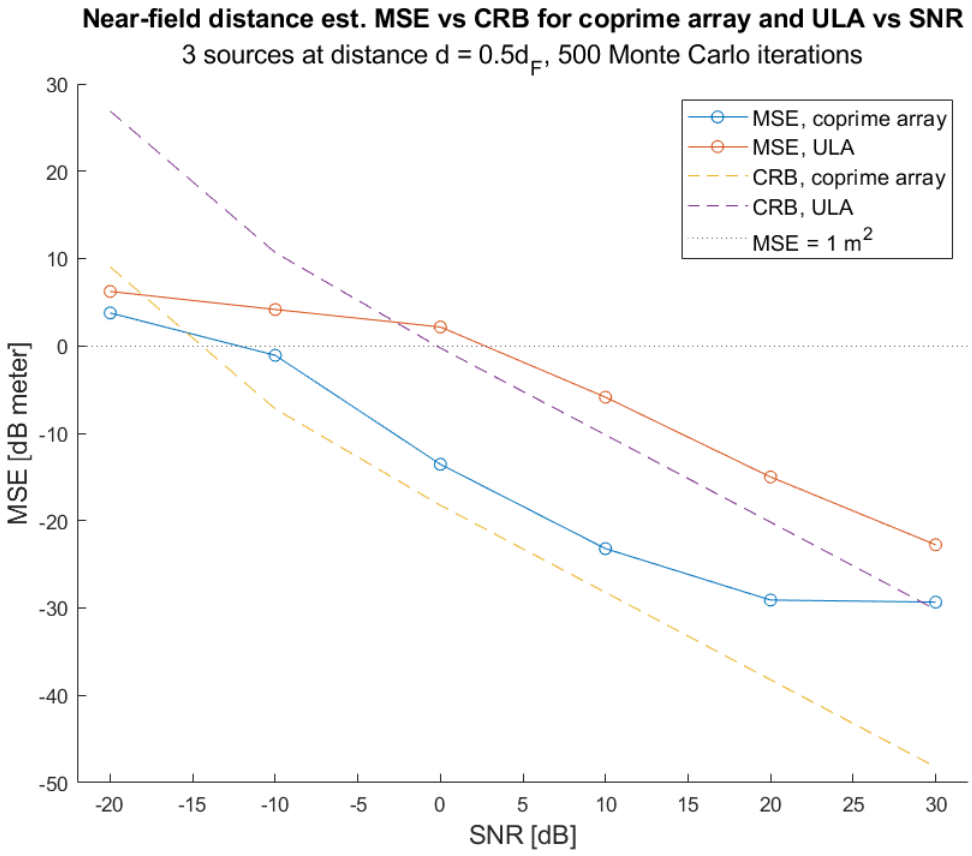

Figure 4.1.2 – Distance estimation accuracy vs signal to noise ratio

It can be seen that for SNR of 0 dB and above both the coprime array and the ULA are able to attain the CRB.

When the SNR is below 0 dB, spurious peaks occasionally can be found in the spatial noise spectrum of the system, causing peak misdetections and a reduction in the system's average accuracy. These peak misdetections are more frequent when dealing with a higher number of sources.

In figure 4.1.2 distance estimation results are shown for the same scenario as before, and the CRB is attained for high SNR values.

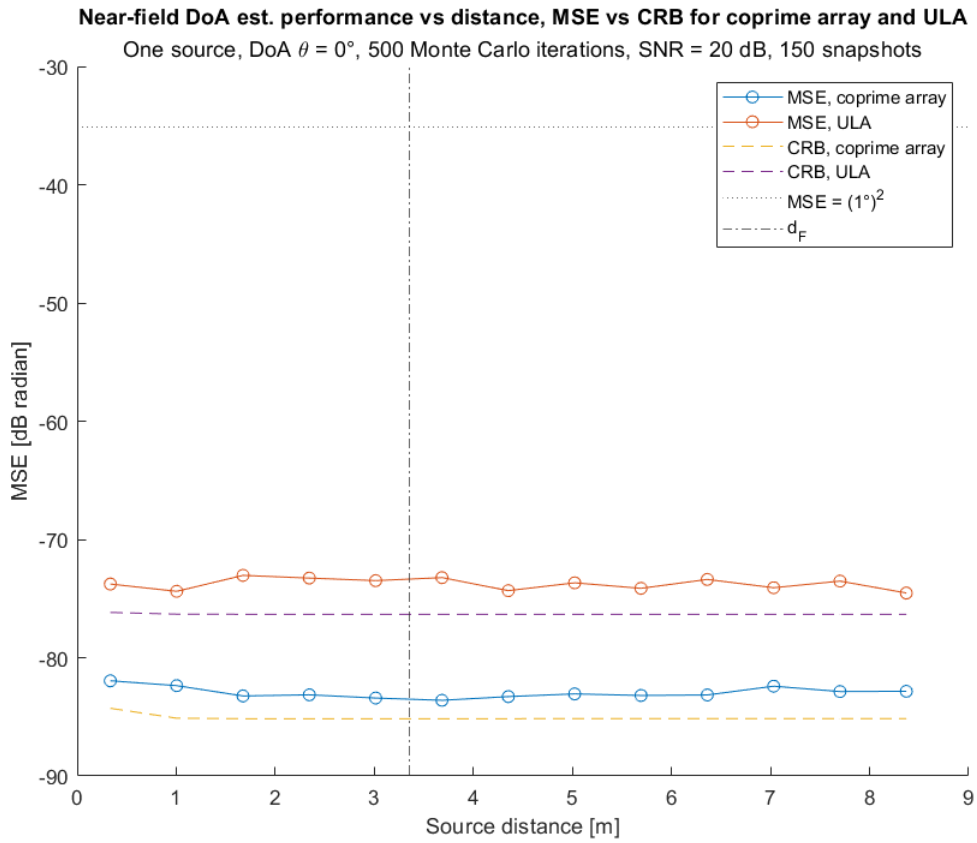

Figure 4.1.3 - DoA estimation accuracy vs distance

For lower SNR values it can be seen that there is a saturation of distance estimation error, that is caused by the limited dimension of the search grid. In fact, with this peak search method the peaks are bound to be located in the grid that has to be specified in advance, limiting therefore the maximum error that can be attained in unfavorable settings such as with a low SNR.

In figure 4.1.3 the simulation results for direction of arrival estimation for a single source with varying distance are shown.

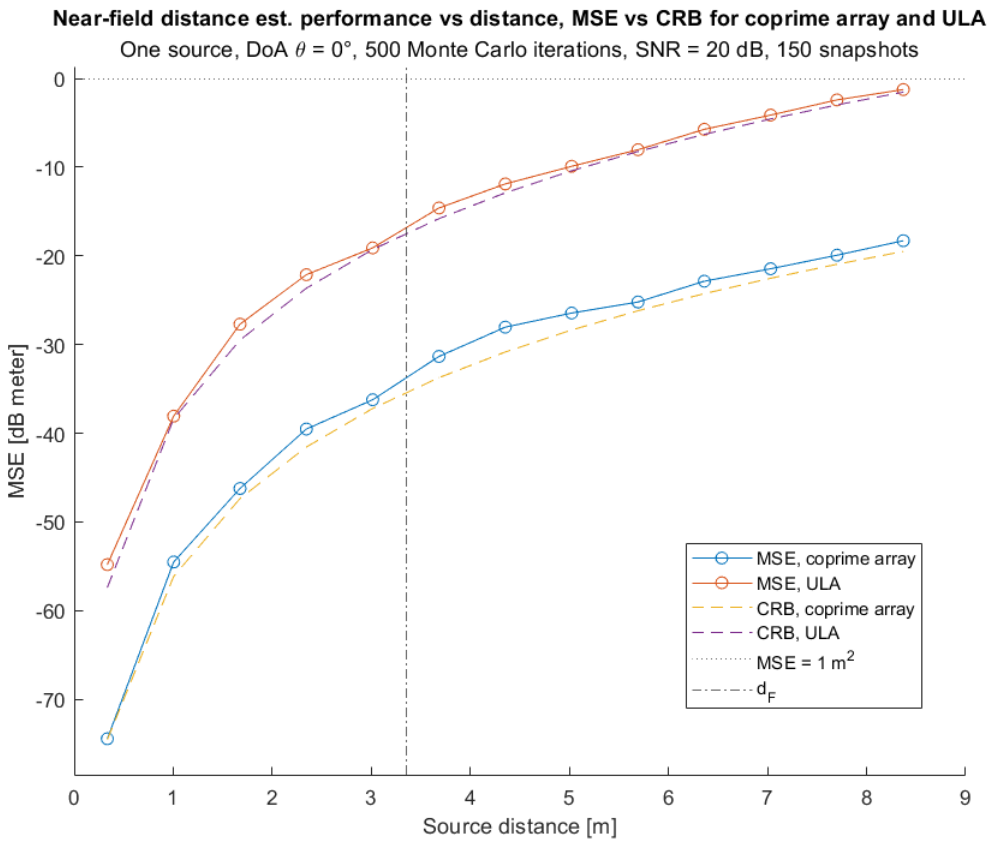

Figure 4.1.4 - Distance estimation accuracy vs distance

It can be seen that the system consistently attains the CRB, and that the MSE does not vary significantly with distance, and that the DoA estimation is accurate both in the near-field and in the far-field of the antenna array.

In figure 4.1.4 the distance estimation's results are presented for the same setting as before.

In this case the system is able to attain the CRB, but the accuracy drops significantly for sources in the far-field, making the distance estimation error the prevailing component of the total position estimation error.

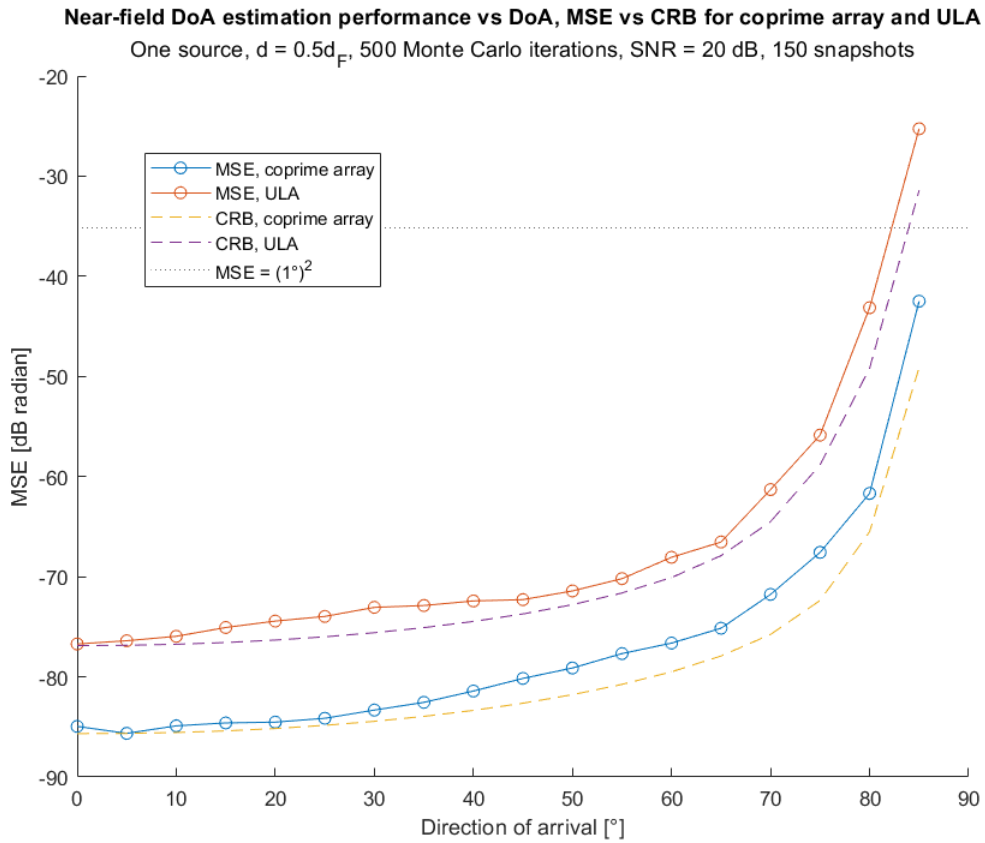

Figure 4.1.5 - DoA estimation accuracy vs source direction

This fact can be attributed to geometrical factors, as pointed out in previous parts of this thesis.

Figure 4.1.5 details the system's direction of arrival estimation performance for a single source with varying impinging angle, a distance of $d = 0.5d_F$, $SNR = 20\ dB$, and a total of 150 snapshots.

The CRB is consistently attained, and the MSE grows larger for more angled sources, as the effective aperture gets lower.

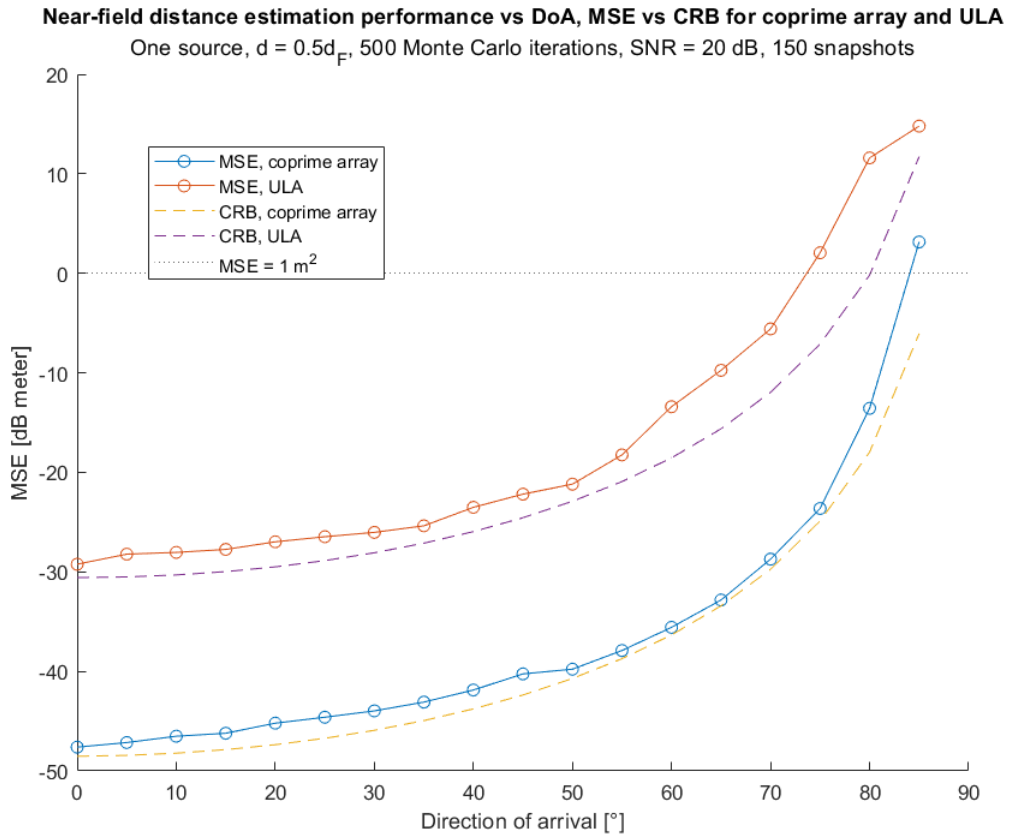

Figure 4.1.6 - Distance estimation accuracy vs source direction

In figure 4.1.6, the distance estimation results for the same setting are shown. The system attains CRB, and the coprime array outperforms the ULA by roughly 20 dB, a conspicuous difference that can be attributed to the larger near-field zone of the coprime over the ULA.

Figure 4.1.7 shows the direction of arrival estimation perfomance for a varying number of source. The simulation is carried out with $SNR = 20\,dB$, sources evenly spaced in the $[-60°. 60°]$ interval, distance $d = 0.5d_F$ from the origin and 150 snapshots.

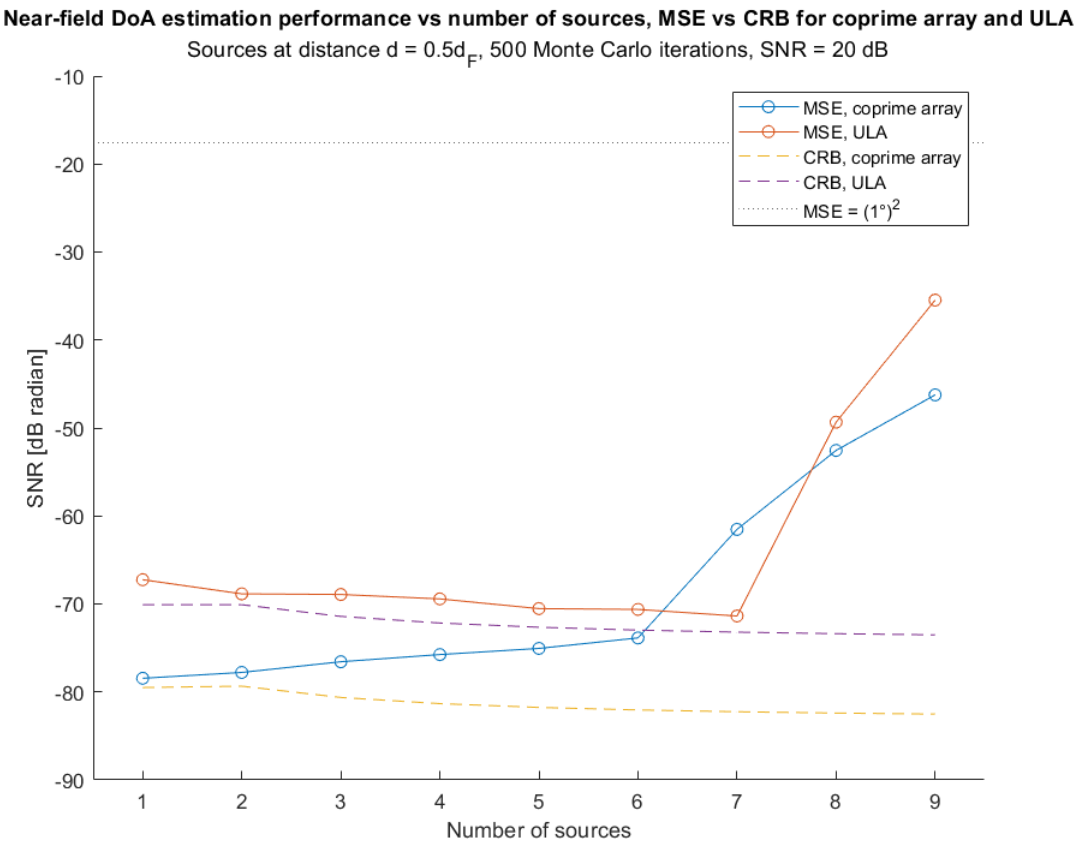

Figure 4.1.7 - DoA estimation accuracy vs number of sources

The simulation is carried out for a number of sources that ranges between 1 and 9, the latter being the greatest number of sources that can be solved with this method by a 10 elements array.

Both for the coprime array and the ULA the accuracy drops when the number of sources exceeds half the number of antenna elements, since the estimation is carried out on the spatial noise spectrum of the received signal.

Similar results can be observed in figure 4.1.8, that concerns distance estimation in the same setting.

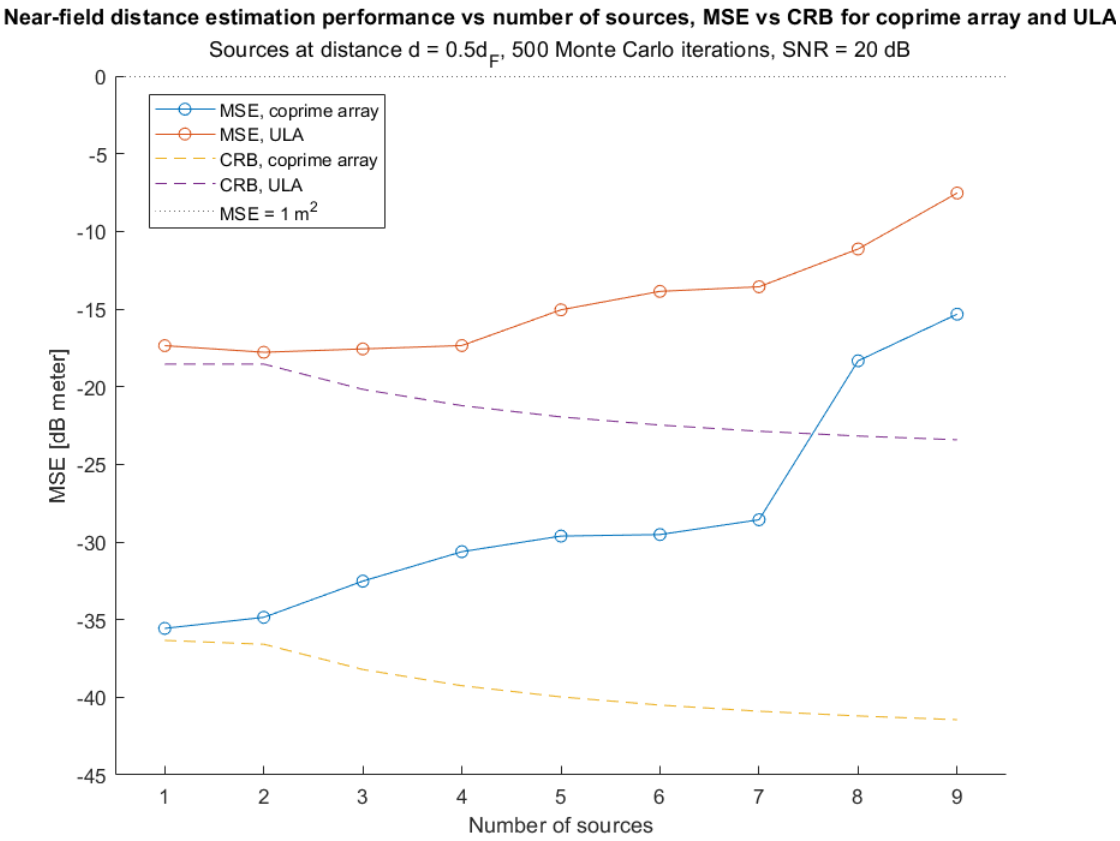

Figure 4.1.8 - Distance estimation accuracy vs number of sources

The CRB is most precisely attained for a low number of sources, and the MSE-CRB gap widens for an increasing amount of sources.

From a practical point of view, this results can be interpreted as the fact that the theoretical amount degrees of freedom isn't attainable with accuracy, therefore in practice it's better to have more element than strictly needed based on the DoFs.

In figure 4.1.9 the direction of arrival performance are shown for a varying number of snapshots.

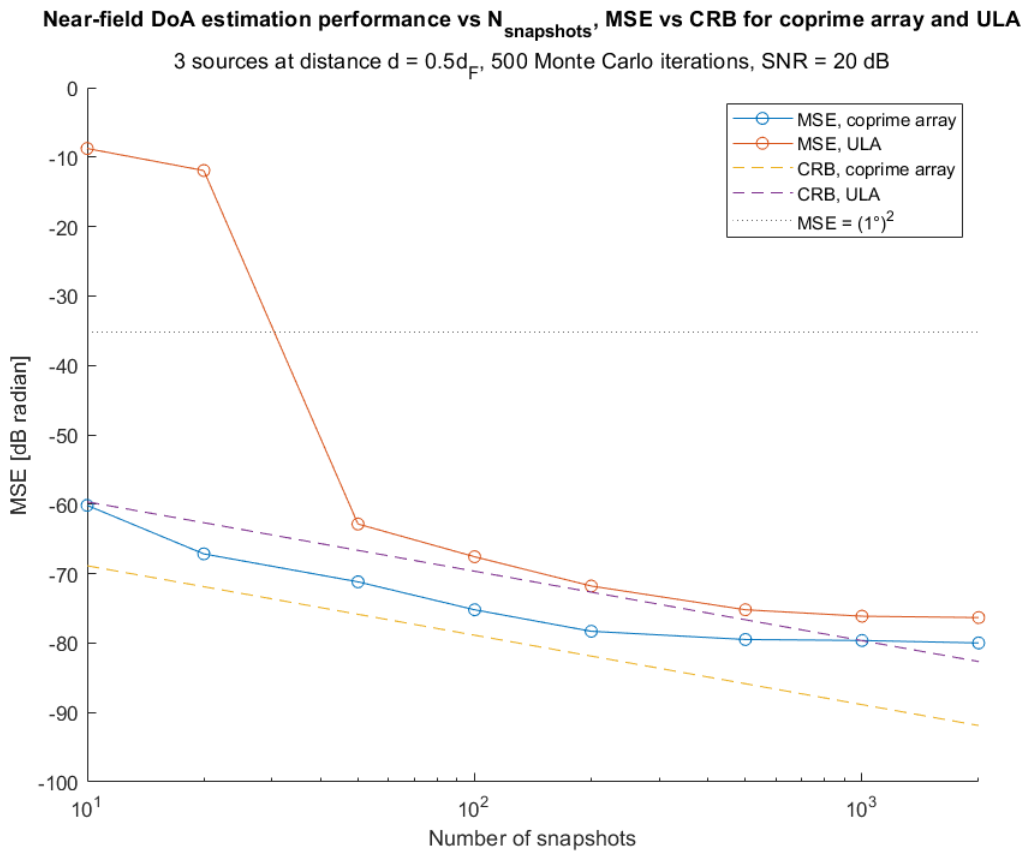

Figure 4.1.9 - DoA estimation accuracy vs number of snapshots

In this simulation there are 3 sources with distance $d = 0.5d_F$ and direction of arrival $\{-60°, 0°, 60°\}$, SNR is 20 dB and 500 Monte Carlo iterations are performed. The simulation is carried out for number of snapshots in the set $\{10, 20, 50, 100, 200, 500, 1000, 2000\}$.

The coprime array attains the CRB, but a saturation effect is present for high number of snapshots, in which increasing the number of snapshots doesn't yield a lower MSE in the DoA estimation.

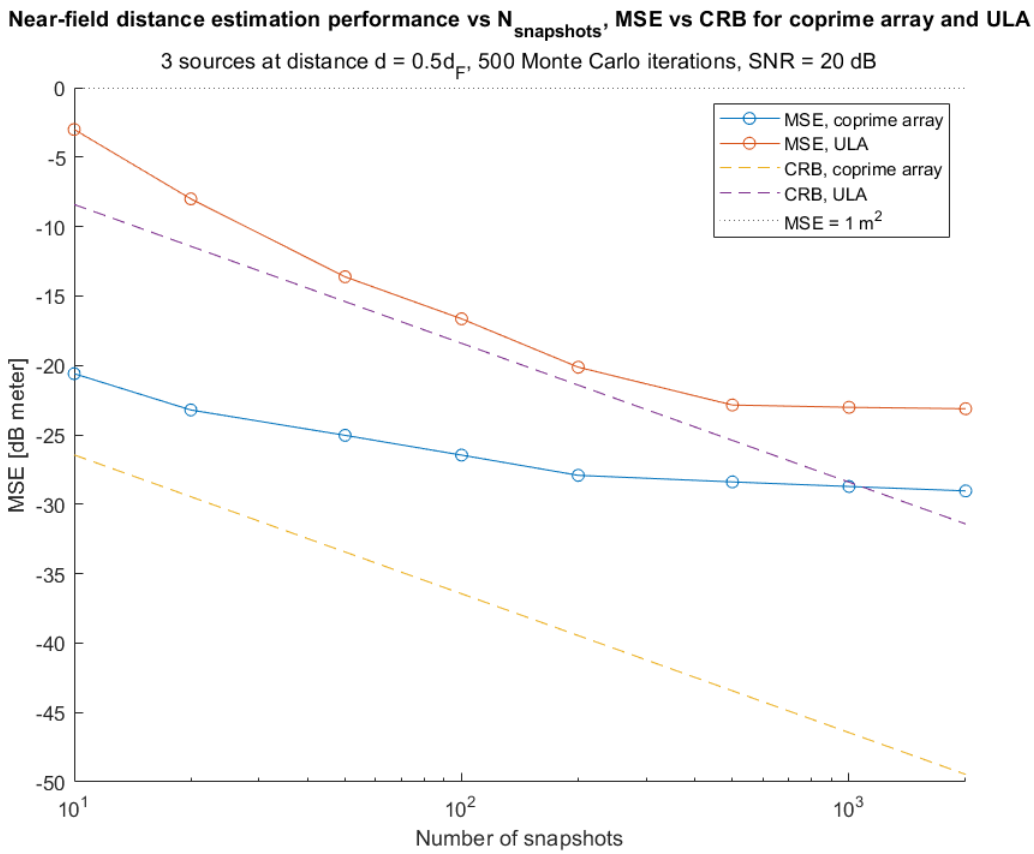

Figure 4.1.10 - Distance estimation performance vs number of snapshots

In figure 4.1.10 the distance estimation performance is detailed for varying number of snapshots and the same setting.

A similar saturation effect can be observed, suggesting that there is an optimal number of snapshots above which there isn't an increase in performance, but only an increase in total acquisition time, since snapshots are taken at intervals that are inversely proportional to the signal bandwidth.

In figure 4.1.11 the resolution of the system is evaluated: two sources are closely spaced with directions of arrival that have varying difference and are

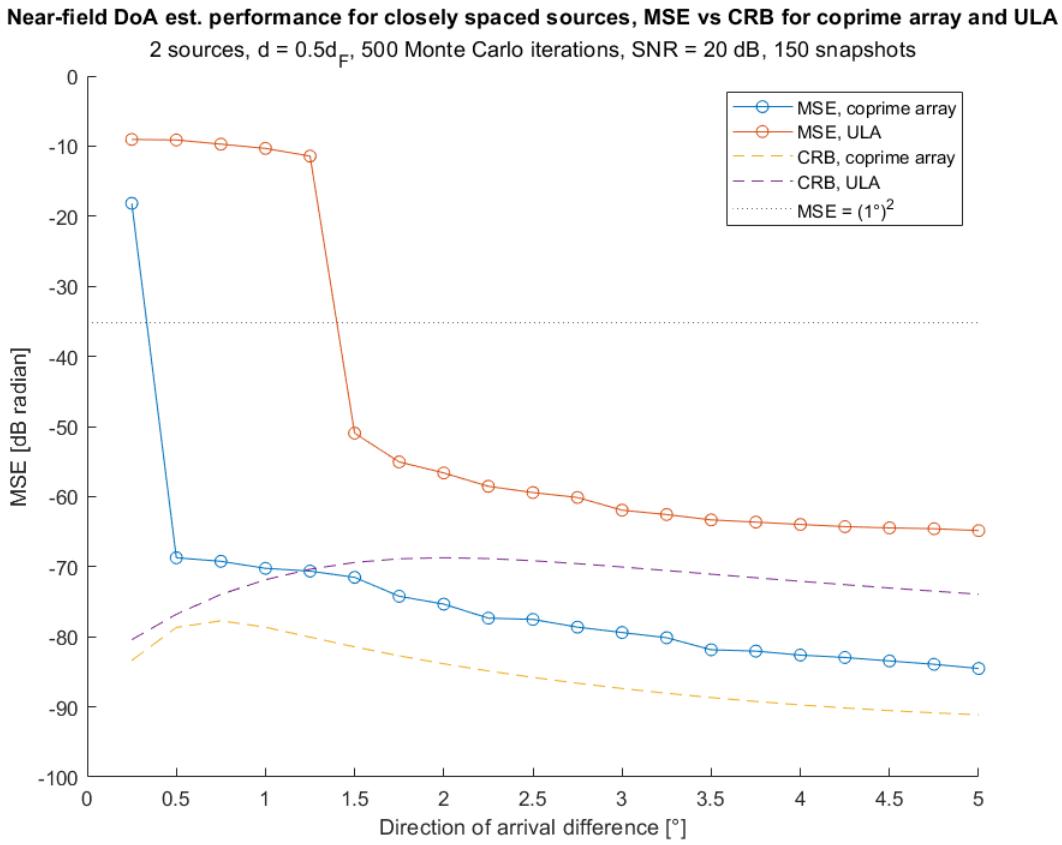

Figure 4.1.11 - DoA estimation performance with closely spaced sources

centered in 0°. The two sources have a distance $d = 0.5d_F$, the SNR is set to 20 dB, 500 Monte Carlo iterations are performed and 150 snapshots are taken.

The coprime array is able to tell apart sources that have a smaller difference in DoA because of the higher aperture of this topology w.r.t the ULA. When the difference of DoA goes above the arrays' respective resolution, that can be estimated to be of 0.5° and 1.5° respectively for the coprime array and the ULA, the CRB is attained as shown in previous simulations' results.

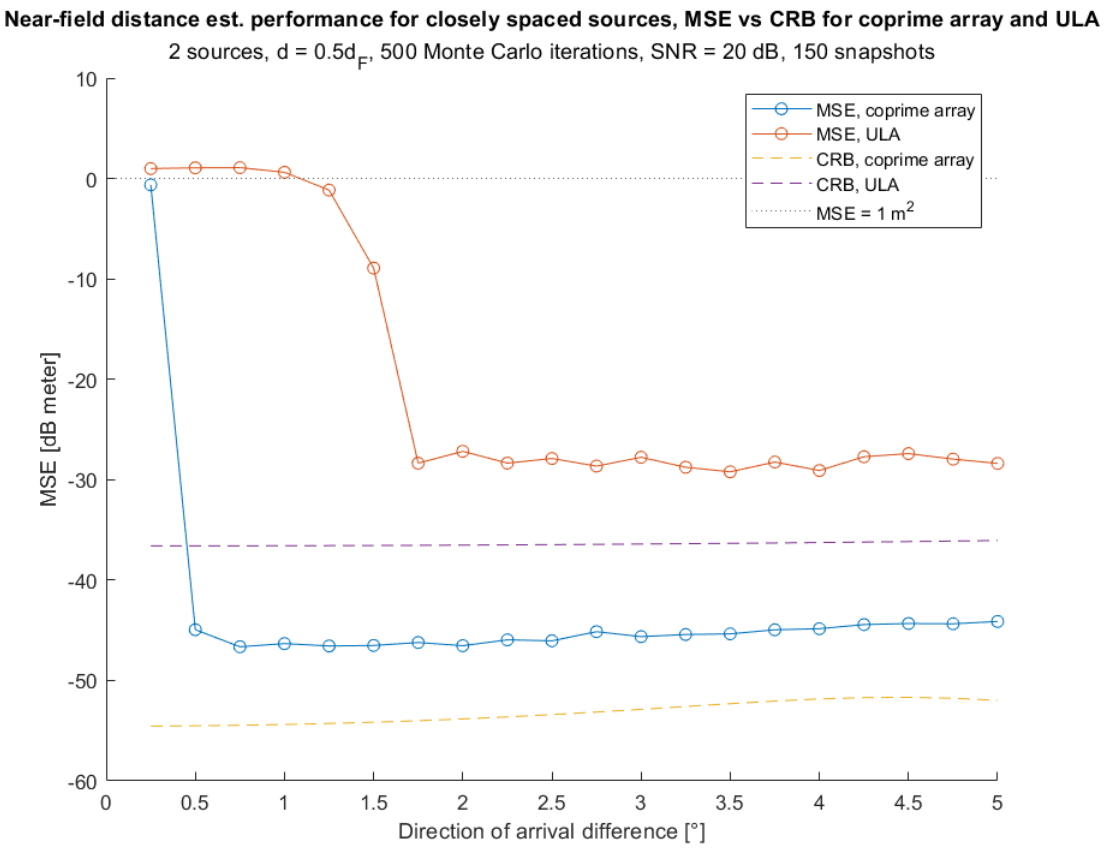

Figure 4.1.12 - Distance estimation performance for closely spaced sources

In figure 4.1.12 the results for the distance estimation are shown for the same setting.

The results are qualitatively similar to those of the DoA estimation, as the minimum DoA difference required in order for the system to tell apart the sources is analogous.

4.2 Noise spatial spectrum

In this subsection, the noise spatial spectrum of the coprime array are shown for several situations, showing how, by varying the system's parameters different results are achieved.

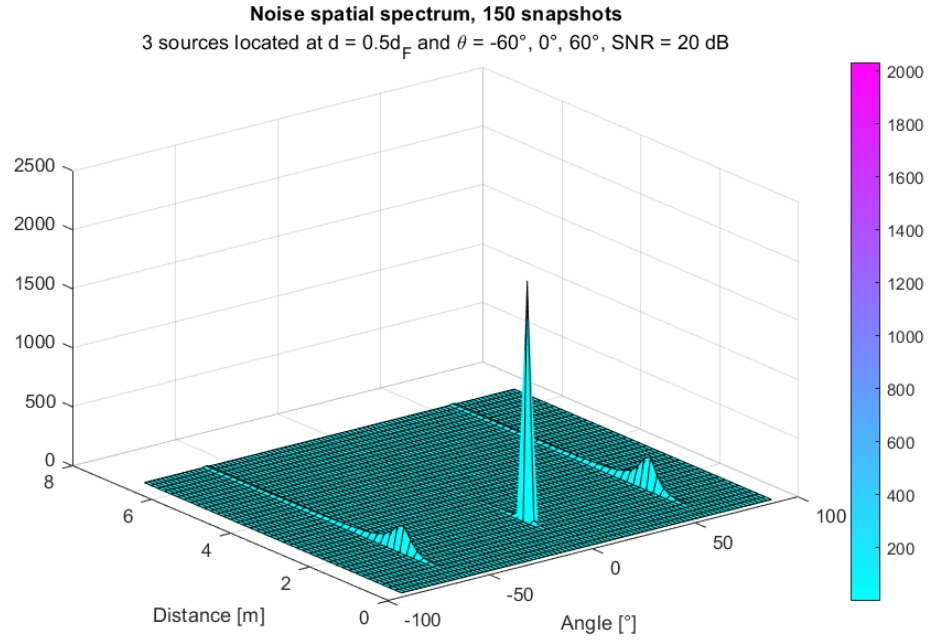

Figure 4.2.1 - Noise spatial spectrum

In figure 4.2.1 the spatial spectrum for 3 sources located in the near-field of the coprime array is shown.

The three peaks corresponding to the sources' locations are clearly discernible, and these peaks are defined more narrowly in the angular dimension rather than

in the distance dimension, due to the different accuracy of the estimator in these two dimensions that has hitherto outlined.

In figure 4.2.2 the same scenario as before has been simulated, but with a small number of snapshots.

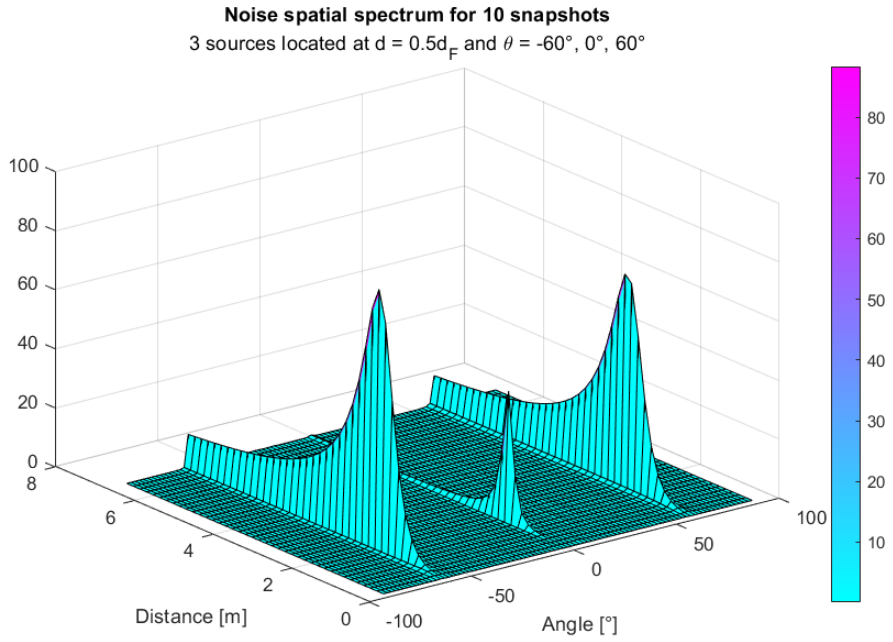

Figure 4.2.2 - Noise spatial spectrum, small number of snapshots

It can be seen how the peaks tails are broader in this case, due to the sample covariance matrix of the system having been estimated from a smaller number of snapshots. This leads to less accurate direction of arrival and distance estimation performance.

The opposite happens in figure 4.2.3, where the number of snapshots taken is increased to 500, leading to narrow tails of the noise spectrum, therefore to more accurate estimation.

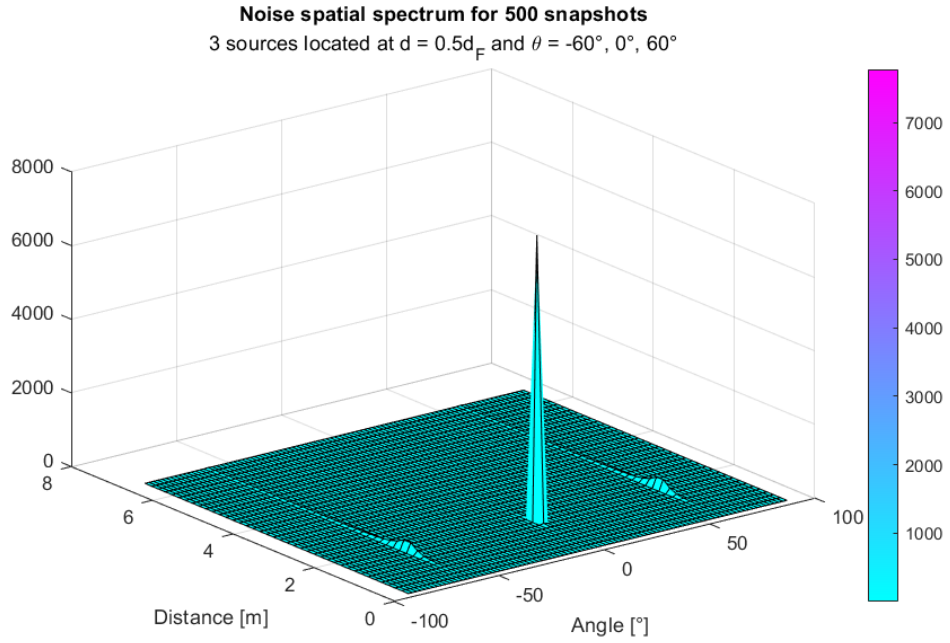

Figure 4.2.3 - Noise spatial spectrum, high number of snapshots

With an increased number of sources transmitting to the array, such as in figure 4.2.4, the estimation is less accurate, and even though peaks are still clearly discernible by the peak search algorithm, the presence of spurious peaks can be noted.

These spurious peaks can lead to sources' misdetections, vastly increasing the MSE of the DoA and distance estimation. When more snapshots are taken by the system the risk of misdetections reduces, being the received signals' covariance matrix a closer estimate of the true covariance matrix of the random process generating the stochastic signal.

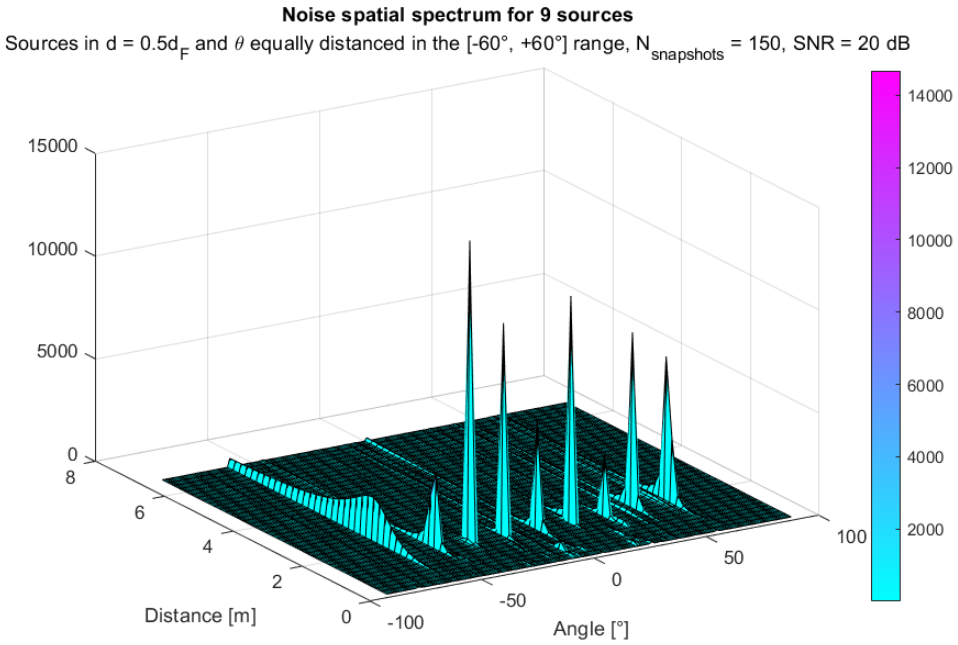

Figure 4.2.4 - Noise spatial spectrum, high number of sources

In figure 4.2.5 the noise spectrum is shown for a source impinging from an angle $\theta = 75°$.

The tails of the peak are particularly elongated both in the angular and in the distance dimension, leading to less accurate estimation due to the lower effective aperture seen by the source, coherently with the experimental results previously illustrated.

In figure 4.2.6 the noise spectrum is shown for a source in the far-field of the array, as the distance is $d = 2.5d_F$.

Coherently with the previous results, the peak is narrowly defined in the angular dimension, albeit it shows elongated tails in the distance dimension, that make the distance estimation less accurate.

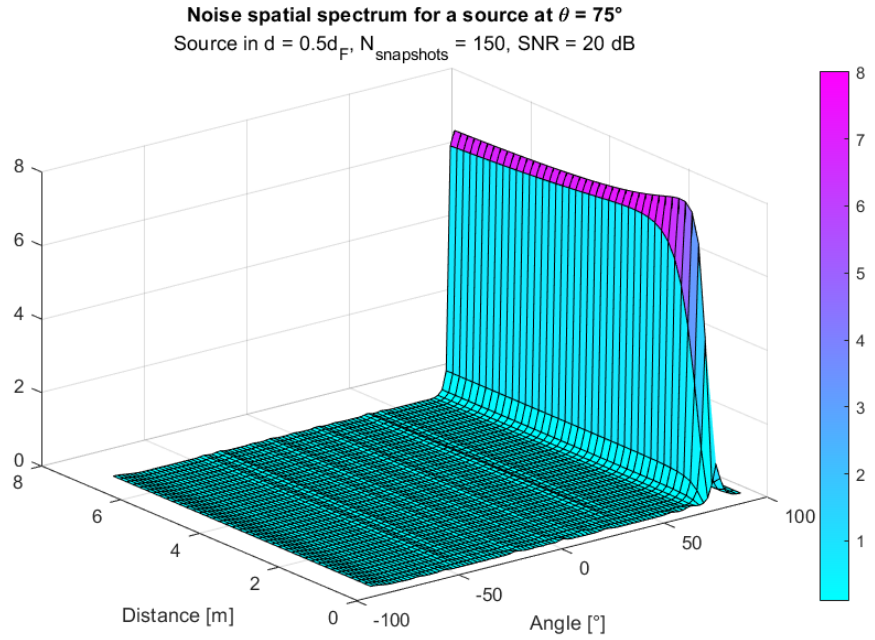

Figure 4.2.5 - Noise spatial spectrum, heavily angled source

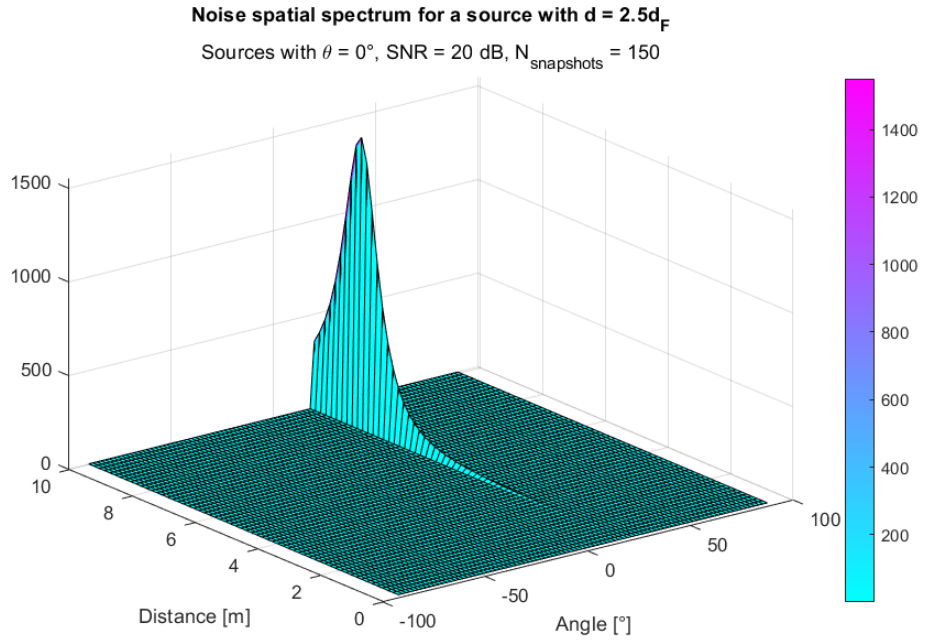

Figure 4.2.6 - Noise spatial spectrum, source in the far-field of the array

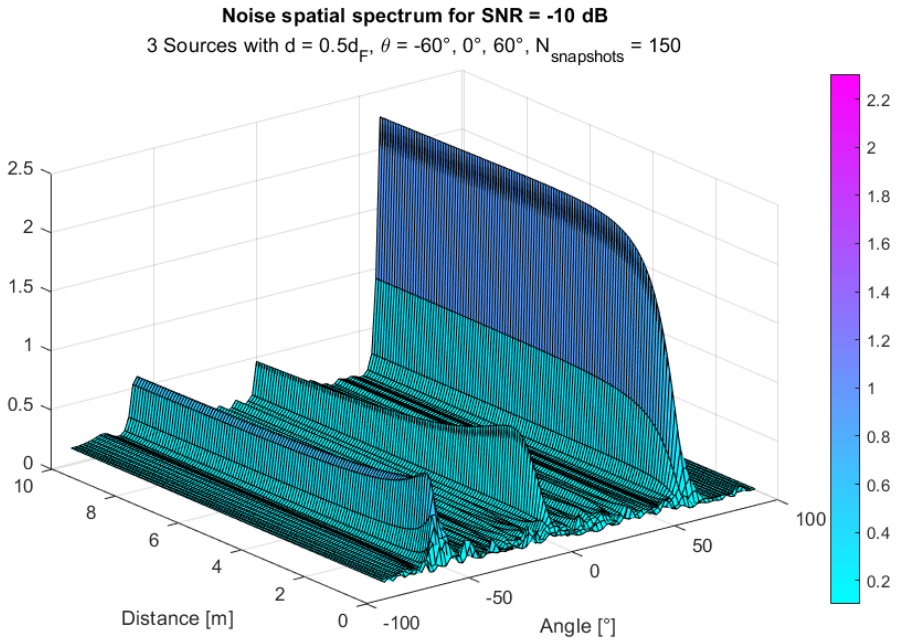

Figure 4.2.7 - Noise spatial spectrum, low SNR situation

Lastly, in figure 4.2.7 the spatial spectrum is shown in a low (-10 dB) signal to noise ratio.

Three sources lie at the same distance of $d = 0.5d_F$, but in the noise spectrum the peaks are not clearly discernible because of the high noise component. In addition to that, spurious peaks are present in low SNR scenarios, especially in the immediate proximity of the coprime array, making the probability of peak misdetection higher.

4.3 Localization accuracy for large arrays

The results presented to this point revolve around the use of a 10 elements coprime array, that has a Fraunhofer distance $d_F = 3.3482m$. Being able to perform positioning in such a narrow radius is an application of scarce interest in real life applications, but the estimation performance previously presented can be generalized for larger arrays.

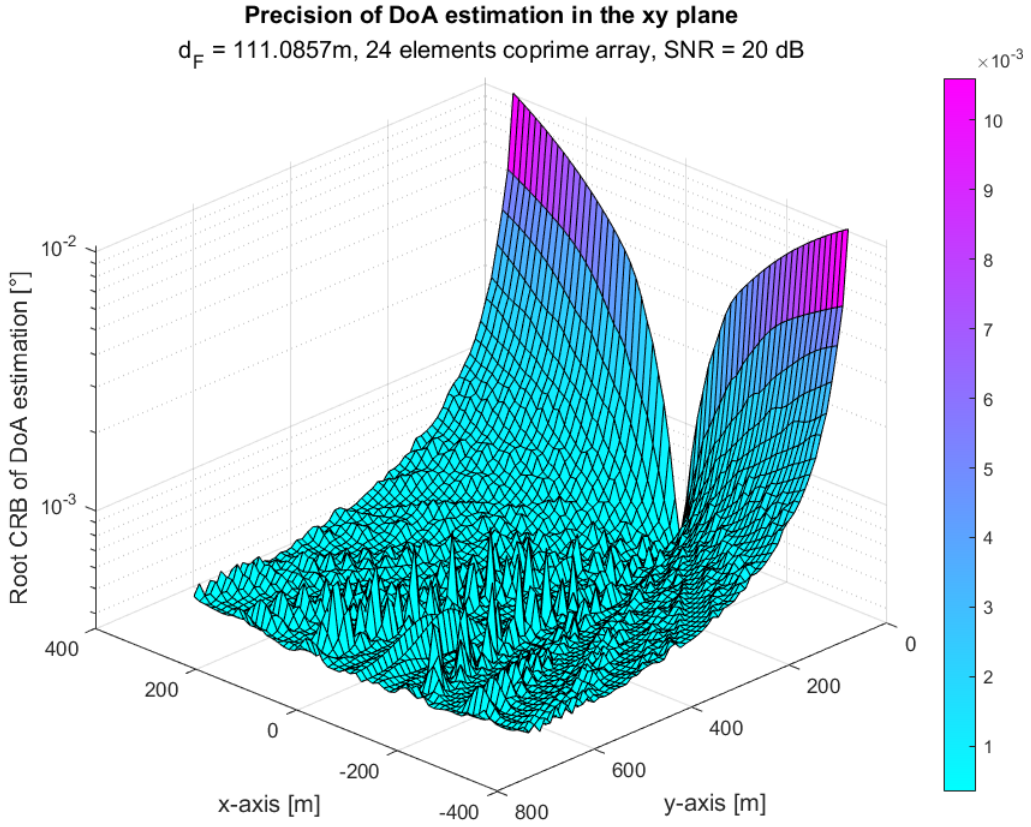

Figure 4.3.1 - Direction of arrival estimation accuracy for a larger array, log scale

As shown in figure 1.1.1, arrays consisting of more elements have a larger Fraunhofer distances, therefore being able to perform accurate positioning both in DoA and in distance in a wider area.

Figure 4.3.1 shows, for a 24 elements coprime array having a Fraunhofer distance $d_F = 111.0857m$ and an aperture of $0.7714m$, the root of the Cramér-Rao bound on the direction of arrival estimation for sources in different position. It can be appreciated how the system is able to accurately estimate the DoA in a wide area, exception made for very angled sources.

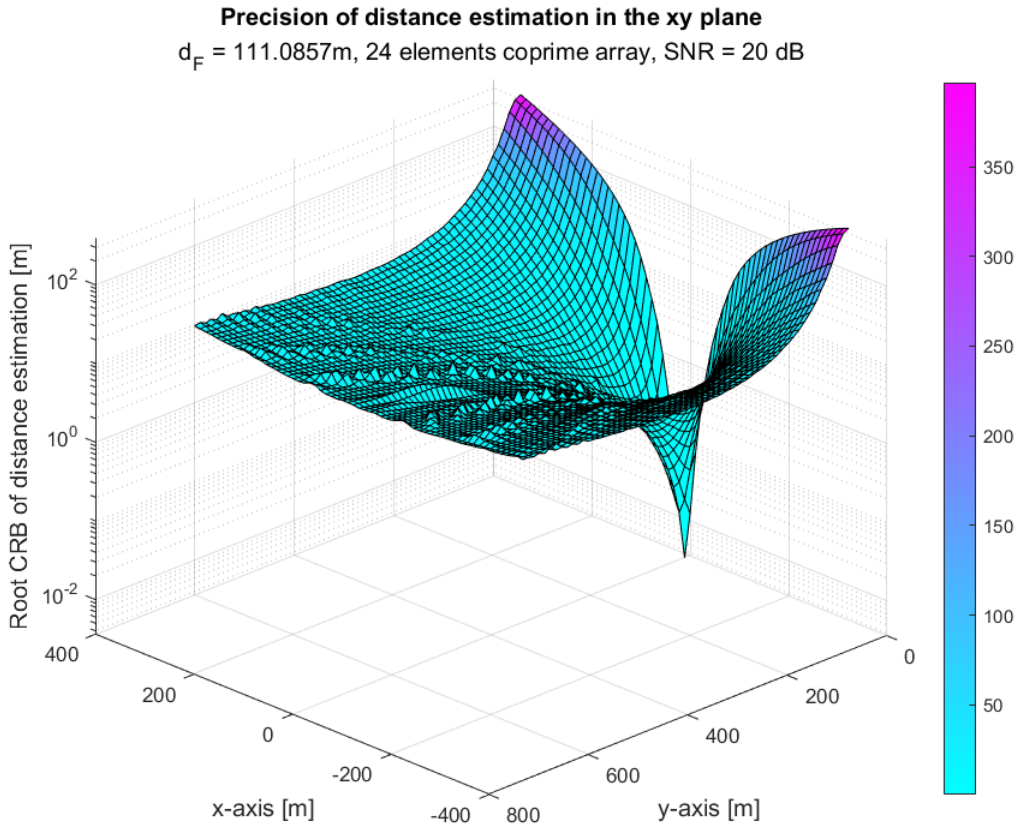

Figure 4.3.2 - Distance estimation accuracy for a larger array, log scale

Correspondingly, figure 4.3.2 shows the distance estimation root CRB for a source located in different positions around a 24 elements coprime array.

Very angled sources have a low distance estimation accuracy, and this accuracy also decreases for sources in the far-field of the array.

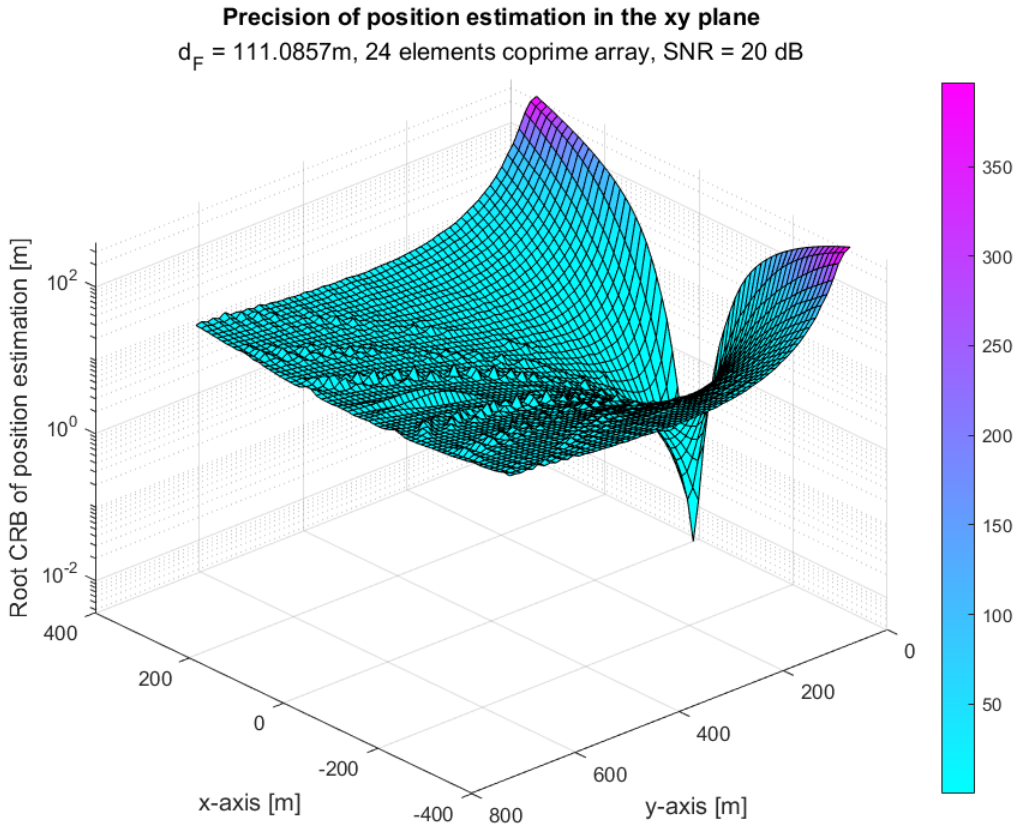

Figure 4.3.3 - Position estimation accuracy for a larger array, log scale

The estimated DoA and distance represent the source's position in polar coordinates in the xy plane, therefore in figure 4.3.3 the total position accuracy is shown.

This position estimation's root CRB is computed by combining, via the Pythagoras' theorem the radial uncertainty on position derived from the distance estimation with the tangential uncertainty derived from the direction of arrival esitimation.

Of these two components that form the position estimation root CRB the predominant one is the one relative to the distance estimation, since it has been shown repeatedly how this estimation is less precise than the DoA one. In fact, figure 4.3.2 and figure 4.3.3 are practically indiscernible from one another.

Chapter 5

Conclusions

This thesis has presented a method to reliably estimate the position of a source in the near-field of a coprime array, that is based on modifications of geometrical nature of the popular MUSIC algorithm. These modifications account for the different source-antenna distances and angles that characterize sources in the near-field of an array.

The CRB that has been analytically derived for this setting shows the strength of the method, while at the same time being suited for computing the accuracy with other sparse array topologies.

The sparse nature of the spatial noise spectrum poses the need for iterative peak search methods, and in choosing the granularity of the initial search grid there is a trade-off between computational time and ability of resolving closely spaced sources.

Practical results express the potentiality of this method to estimate the position in a large radius around the array using a limited size array, as an array of less than a meter is able to accurately locate sources in several hundreds of meters.

The presented method is able to resolve less sources than array elements: difference-coarray domain methods can overcome this limit, similar developements in the near-field of the array would represent an improvement over this method, albeit at a superior computational cost.

Acronyms and notation

λ: carrier wavelength;

σ_n^2: noise power;

$\boldsymbol{\sigma}_s^2$: transmitted source power;

θ: the impinging wave angle;

$\circ$: Hadamard (elementwise) matrix product;

$\otimes$: Kronecker matrix product;

$\boldsymbol{A}$: steering matrix of the array;

B: bandwidth;

CRB: Cramér-Rao Bound;

D: array aperture;

D_{eff}: effective array aperture;

d_e: inter-element spacing;

d_F: Fraunhofer distance;

DoA: Direction of Arrival;

DoF(s): Degree(s) of Freedom;

f_0: central frequency;

FIM: Fisher Information Matrix;

GDOP: Geometric Dilution of Precision;

HPBW: Half power beamwidth;

K: number of sources;

$\boldsymbol{n}(t)$: noise;

$\boldsymbol{n_e}$: integer array elements' positions;

MSE: Mean squared error;

MUSIC: Multiple SIgnal Classification;

$\mathcal{N}()$: nullspace, or kernel;

$\widehat{\boldsymbol{Q}}_{\boldsymbol{S}}, \widehat{\boldsymbol{Q}}_{\boldsymbol{N}}$: signal/noise associated eigenvectors matrix;

$\mathcal{R}()$: linear span of a set of vectors;

$\boldsymbol{R_y}, \widehat{\boldsymbol{R}}_{\boldsymbol{y}}$: Covariance matrix, sample covariance matrix;

$\boldsymbol{s}(t)$: signal transmitted by the sources;

$\mathcal{S}_N$: noise spatial spectrum of the received signals;

$\mathcal{S}_S$: signal spatial spectrum of the received signals;

SNR: signal to noise ratio;

T: number of snapshots;

ULA: Uniform Linear Array;

$vec()$: vectorization operation (on a matrix);

w.r.t.: with respect to;

$\boldsymbol{y}(t)$: signal received by the array;

Bibliography

[1] Schmidt R. (1979) Multiple emitter location and signal parameter estimation. Proceedings of RADC spectrum estimation workshop, Saxpy Computer Corporation, USA, 243-258.

[2] J. Sherman, "Properties of focused apertures in the fresnel region," in IRE Transactions on Antennas and Propagation, vol. 10, no. 4, pp. 399-408, July 1962, doi: 10.1109/TAP.1962.1137900.

[3] B. Friedlander, "Localization of Signals in the Near-Field of an Antenna Array," in IEEE Transactions on Signal Processing, vol. 67, no. 15, pp. 3885-3893, 1 Aug.1, 2019, doi: 10.1109/TSP.2019.2923164.

[4] U. Spagnolini, Statistical Signal Processing in Engineering; John Wiley & Sons: Hoboken, NJ, USA, 2018;

[5] B. D. Van Veen and K. M. Buckley, "Beamforming: a versatile approach to spatial filtering," in IEEE ASSP Magazine, vol. 5, no. 2, pp. 4-24, April 1988, doi: 10.1109/53.665.

[6] P. P. Vaidyanathan and P. Pal, "Direct-MUSIC on sparse arrays," 2012 International Conference on Signal Processing and Communications (SPCOM), Bangalore, India, 2012, pp. 1-5, doi: 10.1109/SPCOM.2012.6289992.

[7] C. Zhou, Y. Gu, X. Fan, Z. Shi, G. Mao and Y. D. Zhang, "Direction-of-Arrival Estimation for Coprime Array via Virtual Array Interpolation," in IEEE Transactions on Signal Processing, vol. 66, no. 22, pp. 5956-5971, 15 Nov.15, 2018, doi: 10.1109/TSP.2018.2872012.

[8] Hinich, M.J. Processing spatially aliased arrays. J. Acoust. Soc. Am. 1978, 64, 792–794.

[9] Zhiqiang Qiu, Ziyuan He and Mantang Cui, "A method for signal source number estimation based on MUSIC algorithm," 2015 IEEE International Conference on Communication Problem-Solving (ICCP), Guilin, China, 2015, pp. 344-346, doi: 10.1109/ICCPS.2015.7454169.

[10] Harald Cramér (1946) A contribution to the theory of statistical estimation, Scandinavian Actuarial Journal, 1946:1, 85-94, DOI: 10.1080/03461238.1946.10419631

[11] Radhakrishna Rao, C. (1945) Information and accuracy attainable in the estimation of statistical parameters Bulletin of the Calcutta Mathematical Society, 37 (3). pp. 81-91. ISSN 0008-0659

[12] R. A. Fisher, ”On the mathematical foundations of theoretical statistics” Philosoph. Trans. Roy. Soc. London, vol. 222, pp. 309–368, Jan. 19

[13] P. Stoica and A. Nehorai, "MUSIC, maximum likelihood, and Cramér-Rao bound," in IEEE Transactions on Acoustics, Speech, and Signal Processing, vol. 37, no. 5, pp. 720-741, May 1989, doi: 10.1109/29.17564.

[14] Chun-Lin Liu, P.P. Vaidyanathan, Cramér–Rao bounds for coprime and other sparse arrays, which find more sources than sensors, Digital Signal Processing, Volume 61, 2017, Pages 43-61, ISSN 1051-2004, https://doi.org/10.1016/j.dsp.2016.04.011.

[15] H. Lütkepohl, Handbook of Matrices, John Wiley & Sons, 1996.

Appendix A

In order to estimate the Cramér Rao bound for the joint estimation of the DoA and distance of a source in the near field of a linear invertible array the first step is that of computing the Fisher Information matrix.

Therefore we take a $2K \times 1$ parameter vector:

$$\boldsymbol{\xi} = [\theta_1, \dots, \theta_K, d_1, \dots, d_K]^T$$

The FIM is a $2K \times 2K$ matrix whose element at i-th row and j-th column is:

$$\boldsymbol{FIM}[i,j] = T\ tr\left(\boldsymbol{R_y^{-1}} \frac{\partial \boldsymbol{R_y}}{\partial \boldsymbol{\xi}[i]} \boldsymbol{R_y^{-1}} \frac{\partial \boldsymbol{R_y}}{\partial \boldsymbol{\xi}[j]}\right)$$

$$= T\ tr\left(\frac{\partial \boldsymbol{R_y}}{\partial \boldsymbol{\xi}[i]} \boldsymbol{R_y^{-1}} \frac{\partial \boldsymbol{R_y}}{\partial \boldsymbol{\xi}[j]} \boldsymbol{R_y^{-1}}\right)$$

$$= T\ vec\left(\frac{\partial \boldsymbol{R_y}}{\partial \boldsymbol{\xi}[i]}^H\right)^H (\boldsymbol{R_y}^{-T} \otimes \boldsymbol{R_y}^{-1}) vec\left(\frac{\partial \boldsymbol{R_y}}{\partial \boldsymbol{\xi}[j]}\right)$$

Since $tr(\boldsymbol{AB}) = tr(\boldsymbol{BA})$, $tr(\boldsymbol{ABCD}) = vec(\boldsymbol{B}^H)^H(\boldsymbol{A}^T \otimes \boldsymbol{C})vec(\boldsymbol{D})$, and $(\boldsymbol{A} \otimes \boldsymbol{B})^{-1} = \boldsymbol{A}^{-1} \otimes \boldsymbol{B}^{-1}$(this last property is verified for nonsingular $\boldsymbol{A}$ and $\boldsymbol{B}$) [14][15].

Since $\boldsymbol{\xi}$ is a vector composed by angles and distances we have two cases:

$$\begin{cases} \dfrac{\partial \boldsymbol{R_y}}{\partial \theta_k} = \dfrac{\partial(\boldsymbol{AR_sA}^H + \sigma_n^2 \boldsymbol{I})}{\partial \theta_k} = \dfrac{\partial \boldsymbol{A}}{\partial \theta_k} \boldsymbol{R_s A}^H + \boldsymbol{AR_s} \dfrac{\partial \boldsymbol{A}}{\partial \theta_k}^H \\ \dfrac{\partial \boldsymbol{R_y}}{\partial d_k} = \dfrac{\partial(\boldsymbol{AR_sA}^H + \sigma_n^2 \boldsymbol{I})}{\partial d_k} = \dfrac{\partial \boldsymbol{A}}{\partial d_k} \boldsymbol{R_s A}^H + \boldsymbol{AR_s} \dfrac{\partial \boldsymbol{A}}{\partial d_k}^H \end{cases}$$

And the elements of the FIM can be of the type:

$$\begin{cases} T\ vec\left(\dfrac{\partial \boldsymbol{R_y}}{\partial \theta_k}^H\right)^H \left(\boldsymbol{R_y}^{-T} \otimes \boldsymbol{R_y}^{-1}\right) vec\left(\dfrac{\partial \boldsymbol{R_y}}{\partial \theta_k}\right) \\ T\ vec\left(\dfrac{\partial \boldsymbol{R_y}}{\partial \theta_k}^H\right)^H \left(\boldsymbol{R_y}^{-T} \otimes \boldsymbol{R_y}^{-1}\right) vec\left(\dfrac{\partial \boldsymbol{R_y}}{\partial d_k}\right) \\ T\ vec\left(\dfrac{\partial \boldsymbol{R_y}}{\partial d_k}^H\right)^H \left(\boldsymbol{R_y}^{-T} \otimes \boldsymbol{R_y}^{-1}\right) vec\left(\dfrac{\partial \boldsymbol{R_y}}{\partial \theta_k}\right) \\ T\ vec\left(\dfrac{\partial \boldsymbol{R_y}}{\partial d_k}^H\right)^H \left(\boldsymbol{R_y}^{-T} \otimes \boldsymbol{R_y}^{-1}\right) vec\left(\dfrac{\partial \boldsymbol{R_y}}{\partial d_k}\right) \end{cases}$$

In order to compute $\partial \boldsymbol{R_y}/\partial \theta_k$ and $\partial \boldsymbol{R_y}/\partial d_k$, the derivatives of the near-field steering matrix $\partial \boldsymbol{A}/\partial \theta_k$ and $\partial \boldsymbol{A}/\partial d_k$ must be computed.

The steering matrix is an $N + M - 1 \times 1$ matrix (instead of an $N + M - 1 \times K$ one, since one source is considered at each time in the CRB computation, but the same procedure can be applied to a $N + M - 1 \times K$ one).

The steering matrix elements can be computed as:

$$\boldsymbol{A}_{ik} = \frac{d_k}{d_{ik}} \exp\left(j2\pi \frac{f_0}{c} d_e n_e[i] \sin(\theta_{ik})\right)$$

Let's assume that $K = 1$ for ease of notation: the results remain valid and relevant for any number of sources.

Since we are dealing with one source the k subscript can be dropped from the notation and we write more simply:

$$\boldsymbol{A}_i = \frac{d}{d_i} \exp\left(j2\pi \frac{f_0}{c} d_e n_e[i] \sin(\theta_i)\right)$$

In which, for a source that has DoA w.r.t. the origin θ and distance from the origin d, θ_i and d_i denote the DoA and distance of the source as seen from the i-th element of the array, and they both are functions of θ and d:

$$\begin{cases} \theta_i = arctan\left(\dfrac{d\,sin(\theta) - x_i}{d\,cos(\theta)}\right) \\ d_i = \sqrt{(d\,sin(\theta) - x_i)^2 + (d\cos(\theta))^2} \end{cases}$$

From which it can be noted that:

$$\lim_{d\to\infty} \theta_i = \lim_{d\to\infty} arctan\left(\frac{d\,sin(\theta) - x_i}{d\,cos(\theta)}\right) = \arctan(\tan(\theta)) = \theta$$

This immediate result is a consequence of far-field model being an asymptotic approximation of the near-field one.

In order to compute $\partial \boldsymbol{A}_i/\partial\theta$ and $\partial \boldsymbol{A}_i/\partial d$ the elementwise derivative of the steering matrix has to be computed w.r.t. the scalar values θ and d; starting with $\partial \boldsymbol{A}_i/\partial\theta$ we have that:

$$\frac{\partial \boldsymbol{A}_i}{\partial\theta} = \left(\frac{\partial}{\partial\theta}\frac{d}{d_i}\right)\exp\left(j2\pi\frac{f_0}{c}d_e n[i]\sin(\theta_i)\right) + \frac{d}{d_i}\left(\frac{\partial}{\partial\theta}\exp\left(j2\pi\frac{f_0}{c}d_e n[i]\sin(\theta_i)\right)\right)$$

$$\frac{\partial}{\partial\theta}\frac{d}{d_i} = \frac{-d\left(\dfrac{\partial d_i}{\partial\theta}\right)}{d_i^2}$$

$$\frac{\partial d_i}{\partial\theta} = \frac{-1}{2d_i}\left(\frac{\partial}{\partial\theta}((d\,sin(\theta) - x_i)^2 + (d\cos(\theta))^2)\right) = \frac{x_i d\,cos(\theta)}{2d_i}$$

$$\frac{\partial}{\partial\theta}\frac{d}{d_i} = \frac{-x_i d^2\,cos(\theta)}{2d_i^3}$$

$$\frac{\partial}{\partial\theta}\exp\left(j2\pi\frac{f_0}{c}d_e n[i]\sin(\theta_i)\right) = j2\pi\frac{f_0}{c}d_e n[i]\exp\left(j2\pi\frac{f_0}{c}d_e n[i]\sin(\theta_i)\right)\frac{\partial}{\partial\theta}\sin(\theta_i)$$

$$\frac{\partial}{\partial\theta}\sin(\theta_i) = \cos(\theta_i)\frac{\partial\theta_i}{\partial\theta}$$

$$\frac{\partial\theta_i}{\partial\theta} = \frac{1}{1+\left(\frac{d\,sin(\theta)-x_i}{d\,cos(\theta)}\right)^2}\frac{d^2sin^2(\theta)+d^2cos^2(\theta)}{d^2cos^2(\theta)}$$

$$= \frac{d^2}{d^2sin^2(\theta)+d^2cos^2(\theta)+x_i^2-2x_i d\,sin(\theta)} = \frac{d^2}{d^2+x_i^2-2x_i d\,sin(\theta)}$$

$$\frac{\partial}{\partial\theta}\sin(\theta_i) = \frac{d^2\cos(\theta_i)}{d^2+x_i^2-2x_i d\,sin(\theta)}$$

$$\frac{\partial}{\partial\theta}\exp\left(j2\pi\frac{f_0}{c}d_e n[i]\sin(\theta_i)\right) = \frac{j2\pi\frac{f_0}{c}d_e n[i]\exp\left(j2\pi\frac{f_0}{c}d_e n[i]\sin(\theta_i)\right)d^2\cos(\theta_i)}{d^2+x_i^2-2x_i d\,sin(\theta)}$$

Therefore we have that:

$$\frac{\partial\boldsymbol{A}_i}{\partial\theta} = \left(\frac{-x_i d^2\,cos(\theta)}{2d_i^3}\right)\exp\left(j2\pi\frac{f_0}{c}d_e n[i]\sin(\theta_i)\right)+\cdots$$

$$\frac{j2\pi\frac{f_0}{c}d_e n[i]\exp\left(j2\pi\frac{f_0}{c}d_e n[i]\sin(\theta_i)\right)d^3\cos(\theta_i)}{d_i(d^2+x_i^2-2x_i d\,sin(\theta))}$$

$$\frac{\partial\boldsymbol{A}_i}{\partial\theta} = \frac{d^2\exp\left(j2\pi\frac{f_0}{c}d_e n[i]\sin(\theta_i)\right)}{d_i}\cdot\ldots$$

$$\ldots\left(\frac{-x_i\,cos(\theta)}{2d_i^2}+\frac{d\cos(\theta_i)\,j2\pi\frac{f_0}{c}d_e n[i]\exp\left(j2\pi\frac{f_0}{c}d_e n[i]\sin(\theta_i)\right)}{d^2+x_i^2-2x_i d\,sin(\theta)}\right)$$

So this is the analytic expression of the derivative of the steering matrix of the array w.r.t. the direction of arrival, as seen from the origin of the xy axes.

The other derivative to be computed is that of the steering matrix w.r.t. the distance of the source from the origin of the xy axes:

$$\frac{\partial \boldsymbol{A}_i}{\partial d} = \left(\frac{\partial}{\partial d}\frac{d}{d_i}\right)\exp\left(j2\pi\frac{f_0}{c}d_e n[i]\sin(\theta_i)\right) + \frac{d}{d_i}\left(\frac{\partial}{\partial d}\exp\left(j2\pi\frac{f_0}{c}d_e n[i]\sin(\theta_i)\right)\right)$$

$$\frac{\partial}{\partial d}\frac{d}{d_i} = \frac{\sqrt{(d\,sin(\theta)-x_i)^2+(d\cos(\theta))^2} - d\frac{\partial d_i}{\partial d}}{(d\,sin(\theta)-x_i)^2+(d\cos(\theta))^2}$$

$$\frac{\partial d_i}{\partial d} = \frac{-\left(2dsin^2(\theta) - 2x_i sin(\theta) + 2dcos^2(\theta)\right)}{2\sqrt{(d\,sin(\theta)-x_i)^2+(d\cos(\theta))^2}}$$

$$= \frac{(x_i sin(\theta) - d)}{\sqrt{(d\,sin(\theta)-x_i)^2+(d\cos(\theta))^2}} = \frac{(x_i sin(\theta) - d)}{d_i}$$

$$\frac{\partial}{\partial d}\frac{d}{d_i} = \frac{\sqrt{(d\,sin(\theta)-x_i)^2+(d\cos(\theta))^2} - d\frac{(x_i sin(\theta) - d)}{d_i}}{(d\,sin(\theta)-x_i)^2+(d\cos(\theta))^2}$$

$$= \frac{d_i^2 - x_i d\,\sin(\theta) + d^2}{d_i^3}$$

$$\frac{\partial}{\partial d}\exp\left(j2\pi\frac{f_0}{c}d_e n[i]\sin(\theta_i)\right) = j2\pi\frac{f_0}{c}d_e n[i]\exp\left(j2\pi\frac{f_0}{c}d_e n[i]\sin(\theta_i)\right)\frac{\partial}{\partial d}\sin(\theta_i)$$

$$\frac{\partial}{\partial d}\sin(\theta_i) = \frac{\partial}{\partial d}\sin\left(arctan\left(\frac{d\,sin(\theta)-x_i}{d\,cos(\theta)}\right)\right)$$

$$= \cos\left(arctan\left(\frac{d\,sin(\theta)-x_i}{d\,cos(\theta)}\right)\right)\frac{\partial \theta_i}{\partial d}$$

$$\frac{\partial \theta_i}{\partial d} = \frac{1}{1 + \left(\frac{d\,sin(\theta) - x_i}{d\,cos(\theta)}\right)^2} \frac{d\,sin(\theta)\,cos(\theta) - cos(\theta)\,(d\,sin(\theta) - x_i)}{d^2 cos^2(\theta)}$$

$$\frac{\partial \theta_i}{\partial d} = \frac{x_i\,cos(\theta)}{d_i^2}$$

$$\frac{\partial}{\partial d}\sin(\theta_i) = \frac{x_i\,cos(\theta)\cos\left(arctan\left(\frac{d\,sin(\theta) - x_i}{d\,cos(\theta)}\right)\right)}{d_i^2}$$

$$\frac{\partial}{\partial d}\exp\left(j2\pi\frac{f_0}{c}d_e n[i]\sin(\theta_i)\right) = \cdots$$

$$j2\pi\frac{f_0}{c}d_e n[i]\exp\left(j2\pi\frac{f_0}{c}d_e n[i]\sin(\theta_i)\right)\frac{x_i\,cos(\theta)}{d_i^2}\cos\left(arctan\left(\frac{d\,sin(\theta) - x_i}{d\,cos(\theta)}\right)\right)$$

$$\frac{\partial \boldsymbol{A}_i}{\partial d} = \left(\frac{\partial}{\partial d}\frac{d}{d_i}\right)\exp\left(j2\pi\frac{f_0}{c}d_e n[i]\sin(\theta_i)\right) + \frac{d}{d_i}\left(\frac{\partial}{\partial d}\exp\left(j2\pi\frac{f_0}{c}d_e n[i]\sin(\theta_i)\right)\right)$$

$$= \frac{d_i^2 - x_i d\sin(\theta) + d^2}{d_i^3}\exp\left(j2\pi\frac{f_0}{c}d_e n[i]\sin(\theta_i)\right) + \cdots$$

$$\frac{d}{d_i}j2\pi\frac{f_0}{c}d_e n[i]\exp\left(j2\pi\frac{f_0}{c}d_e n[i]\sin(\theta_i)\right)\frac{x_i\,cos(\theta)}{d_i^2}\cos\left(arctan\left(\frac{d\,sin(\theta) - x_i}{d\,cos(\theta)}\right)\right)$$

$$\frac{\partial \boldsymbol{A}_i}{\partial d} = \frac{x_i(x_i - sin(\theta))\exp\left(j2\pi\frac{f_0}{c}d_e n[i]\sin(\theta_i)\right)}{d_i^3} + \cdots$$

$$\cdots\frac{x_i d\,j2\pi\frac{f_0}{c}d_e n[i]\exp\left(j2\pi\frac{f_0}{c}d_e n[i]\sin(\theta_i)\right)\cos(\theta_i)\,cos(\theta)}{d_i^3}$$

Once the analytical expressions for the $\partial \boldsymbol{A}_i/\partial\theta$ and $\partial \boldsymbol{A}_i/\partial d$ matrixes are derived are the matrixes $\partial \boldsymbol{R_y}/\partial\theta_k$ and $\partial \boldsymbol{R_y}/\partial d_k$ can be easily computed, and from there

the 2×2 Fisher Information matrix is derived. FIM elements will have higher values for higher number of snapshots and higher signal to noise ratio.

So the $\boldsymbol{CRB}$ is obtained as:

$$\boldsymbol{CRB} = \boldsymbol{FIM}^{-1}$$

And:

$$\begin{cases} CRB(\theta_k) = \boldsymbol{CRB}[i,i] & i \in [1, K] \\ CRB(d_k) = \boldsymbol{CRB}[i,i] & i \in [K+1, 2K] \end{cases}$$

This analytical formulation of the FIM (and consequently of CRB) has the strength of being exact, valid for any number of snapshots, for any signal to noise ratio and for different types array topology, and it's easy to empirically find how the performance of the DoA and distance estimator vary when any of the parameters vary.

This interpretability gives valuable insights on the performance of the estimator when choosing the various parameters that the CRB depends on.